Enhanced nocturnal N_2O_5-$ClNO_2$ chemistry in Delhi under reduced NO conditions

Yijing Chen[1,2], Cheng Wu[2]*, Epameinondas Tsiligiannis[2], Ravi Kant Pathak[2,3], Jan B. C. Pettersson[2], Harsh Raj Mishra[2,3]†, Gazala Habib[4], Geetam Tiwari[5], Kebin He[1], Jingkun Jiang[1]*, Mattias Hallquist[2]*

Affiliations:

[1]State Key Laboratory of Regional Environment and Sustainability, School of Environment, Tsinghua University, Beijing, 100084, China.

[2]Department of Chemistry and Molecular Biology, University of Gothenburg, Gothenburg, 40530, Sweden.

[3]Indo-Gangetic Plains Centre for Air Research and Education (IGP-CARE), Hamirpur, Uttar Pradesh, 210301, India.

[4]Transportation Research and Injury Prevention Centre, Indian Institute of Technology Delhi, New Delhi, 110016, India.

[5]Department of Civil Engineering, Indian Institute of Technology Delhi, New Delhi, 110016, India.

†Present address: School of Earth and Atmospheric Sciences, Queensland University of Technology, Queensland, 4001, Brisbane, Australia.

***Correspondence to:** Mattias Hallquist (hallq@chem.gu.se), Jingkun Jiang (jiangjk@tsinghua.edu.cn) and Cheng Wu (cheng.wu@gu.se).

This PDF file includes:

ABSTRACT.

Nitryl chloride ($ClNO_2$) is an important Cl· precursor, originating from the heterogeneous reactions of dinitrogen pentoxide (N_2O_5) on chloride-containing particles. This N_2O_5-$ClNO_2$ chemical process plays critical roles in chloride activation, nitrate formation, and thus air pollution. Here we present field measurements made in the early springtime of 2023 in Delhi and compare with a previous study conducted during the winter of 2019. We found elevated nocturnal levels of N_2O_5 and $ClNO_2$, averaging 13 and 80 ppt, respectively, which are approximately doubled compared to observations in 2019. This change is primarily driven by the reduced nighttime NO levels, from 124 ± 25 ppb in 2019 to 44 ± 9 ppb in 2023. In addition, the chloride concentration (nighttime average 4.7 μg/m^3) in Delhi is among the highest reported globally, driving efficient conversion of N_2O_5 to $ClNO_2$. Decreased NO and elevated $ClNO_2$ levels lead to higher NO_3· and Cl· production that promote the oxidation of organics. Consistently, we observed increased fractions of gaseous nitrogen- and chlorine-containing organic products and a higher oxidation state of the organic aerosols. Our findings highlight the need for increased attention to atmospheric secondary pollution and stringent anthropogenic chlorine emissions control under reduced NO_x conditions in Delhi.

1 INTRODUCTION

Atmospheric N_2O_5-$ClNO_2$ chemistry refers to the conversion of N_2O_5 to $ClNO_2$ on chloride-containing particles (Finlayson-Pitts et al., 1989), which is ubiquitous worldwide (Wang et al., 2019) and exerts profound impacts on nitrogen budgets (Dentener and Crutzen, 1993), chloride activation (Thornton et al., 2010), and atmospheric oxidative capacity (Simpson et al., 2015;Yang et al., 2022). N_2O_5 is formed from the reaction between NO_3· and NO_2 (R1), and the heterogeneous reactions of N_2O_5 on atmospheric particles produce particulate nitrate and gaseous $ClNO_2$ (R2-R5) (Bertram and Thornton, 2009;Finlayson-Pitts et al., 1989;Behnke et al., 1997;Thornton and Abbatt, 2005;Osthoff et al., 2008). The heterogeneous uptake of N_2O_5 on chloride containing particles is in general the main production mechanism of atmospheric $ClNO_2$, which proceeds rapidly with the aqueous reaction between NO_2^+ and Cl^- (R5). Some studies (Dalton et al., 2023;Margerum et al., 1994) have shown that the aqueous reactions of NO_2^- and HONO with Cl_2, HOCl and NH_2Cl are potential sources of $ClNO_2$, with a reaction rate constant about 3~4 orders of magnitude lower than the reaction between NO_2^+ and Cl^-. Other reactions such as HCl reacting with N_2O_5 on surfaces are not considered due to the relatively slow reaction rate constant (Raff et al., 2009).

$$NO + O_3 \xrightarrow{\text{Products} \leftarrow \text{Organics}} NO_2 \xrightarrow{O_3} NO_3 \cdot \underset{\text{heat}}{\overset{NO_2}{\rightleftharpoons}} N_2O_5 \quad (R1)$$

$$N_2O_5\ (g) \leftrightarrow N_2O_5\ (aq)\ (R2)$$

$$N_2O_5\ (aq) + H_2O\ (l) \leftrightarrow H_2ONO_2^+\ (aq) + NO_3^-\ (aq)\ (R3)$$

$$H_2ONO_2^+\ (aq) + H_2O\ (l) \rightarrow HNO_3\ (aq) + H_3O^+\ (aq)\ (R4)$$

$$H_2ONO_2^+\ (aq) + Cl^-(aq) \rightarrow ClNO_2\ (g) + H_2O\ (l)\ (R5)$$

$ClNO_2$ is rather inert at night and undergoes negligible losses, while it photolyzes to produce Cl· during the daytime (Osthoff et al., 2008). Given the fast photolysis of NO_3· and thermal decomposition of N_2O_5, the N_2O_5 to $ClNO_2$ conversion is expected to happen mainly at night (Brown and Stutz, 2012). The occurrence of this nocturnal chemistry was confirmed by direct field observations of N_2O_5 and $ClNO_2$ in the urban coastal air (Osthoff et al., 2008;Riedel et al., 2012), and later extended to polluted inland areas (Thornton et al., 2010;Phillips et al., 2012;Le Breton et al., 2018a;Ma et al., 2023;Chen et al., 2023), where abundant NO_x and particulate chloride precursors co-exist, with measured nighttime peak mixing ratios consistently up to several parts per billion by volume (ppb), which are about an order of magnitude higher than those observed in the remote polar and marine regions (McNamara et al., 2019;Eger et al., 2019;Kercher et al., 2009).

Delhi is one of the world's most polluted megacities. Intense air pollutant emissions from transport, residential, industrial, and other sources provide abundant precursors (i.e., particulate chloride and NO_x, Fig. S1a, b) for N_2O_5 and $ClNO_2$ production. Previous studies in this region have mainly focused on measurements of chloride using AMS or ACSM (Fig. S2 and Table S1). Observations of gaseous chlorinated species (Mishra et al., 2024;Haslett et al., 2023) remain limited. Several recent modeling studies (Meidan et al., 2022;Soni et al., 2023;Patel et al., 2026) have indicated the potential for substantial $ClNO_2$ production, resulting in concentrations up to several ppb in this region; however, the scarcity of field observations leaves these model predictions largely unvalidated, limiting our ability to quantify the impacts of chlorinated species on O_3 and secondary aerosol formation.

The field measurement conducted in winter 2019 found that nighttime N_2O_5 and $ClNO_2$ levels are rather low in Delhi (Haslett et al., 2023), which is attributed to the extremely high NO concentrations (hundreds of ppb) and the fast reaction rate constant between NO and $NO_3\cdot$ (k_{NO+NO3}, 2.6×10^{-11} cm^3 $molec^{-1}$ s^{-1} at 298 K) (Burkholder et al., 2020), thereby largely quenching nocturnal $NO_3\cdot$ (reaction scheme R1) and limiting subsequent N_2O_5 and $ClNO_2$ production. Notably, the 2019 campaign predominantly captured the extremely polluted episodes during the wintertime in Delhi, with the peak occurrence frequencies of $PM_{2.5}$ (185 $\mu g/m^3$), NO (124 ppb) and chloride (21 $\mu g/m^3$) concentrations largely falling at the high end of the concentration distributions commonly observed during the recent years (Fig. S3b, c, d). Due to the scarcity of field observations, the characteristics of N_2O_5-$ClNO_2$ chemistry outside of such extreme NO and chloride conditions in Delhi remain unclear.

In this work, we present a recent field measurement of N_2O_5, $ClNO_2$ and other relevant inorganic and organic species in both gas and particle-phases during the early springtime of 2023 in Delhi. This timing captures a broader range of NO concentrations (below 0.1 to hundreds of ppb) and chemical conditions, which overlaps with but extends beyond previous studies that primarily focused on the most polluted winter months. We characterize the changes in N_2O_5-$ClNO_2$ chemistry relative to the previous observation in winter 2019 (Haslett et al., 2023) and examine the underlying driving factors and impacts. The field derived kinetic parameter, quantified as the product of N_2O_5 uptake coefficient ($\gamma_{N_2O_5}$) and $ClNO_2$ yield (f_{ClNO_2}), is also estimated and compared to those reported from other atmospheric environments. We find enhanced N_2O_5 production driven by decreased NO concentrations, and the formation of $ClNO_2$ is dependent on the chloride level in Delhi. The product of $\gamma_{N_2O_5}\times f_{ClNO_2}$ (average ~0.2) is at the upper end of the values observed around the world, indicating efficient N_2O_5 conversion to $ClNO_2$ in Delhi. We further investigate the impacts of associated increases in $NO_3\cdot$ and $Cl\cdot$ production rates on the atmospheric oxidation of organics, utilizing concurrent measurements of a wide range of molecular-level organic oxidation products.

2 METHODS

2.1 Field observation overview

The field campaign was performed at the Indian Institute of Technology Delhi campus (IIT Delhi, 28.54°N, 77.19°E; ~230 m above the sea level) from 15 February to 14 March in 2023. The valid dataset collected during the early spring period (2/23-3/14) was used for analysis in this study. IIT Delhi is a representative continental urban site situated at the north-western of Indo-Gangetic Plain, which is frequently affected by intense anthropogenic emissions from biomass and waste burning activities, traffic exhaust, power plants, and industries (Kumar et al., 2022;Bryant et al., 2023;Kashyap et al., 2019;Rai et al., 2020), and potential biogenic emissions from the surrounding vegetations (Fig. S4). All the instruments were installed in an air-conditioned laboratory on the 8th floor, at a sampling height (~30 m) above the local vegetation canopy, and thus the observation is representative of an urban background condition. In addition, considering the high aerosol loading and stable nighttime boundary layer (average nighttime wind speed of 0.6 m/s) in Delhi, N_2O_5 or $ClNO_2$ losses through dry deposition on building surfaces or vegetation are expected to be minor. There were no significant precipitation events during the periods selected for intensive chemical analysis. Consequently, wet deposition was not a significant factor in our nocturnal chemical budget and was omitted from the calculations. Details of the measurement design are found in the supplementary information (Text. S1).

FIGAERO-I$^-$-CIMS. N_2O_5, reactive chlorines, and oxygenated organics were identified as iodide clusters ($M{\cdot}I^-$) by a Filter Inlet for Gases and AEROsols Iodide-Chemical Ionization-Time of Flight Mass Spectrometer (FIGAERO-I$^-$-HR-ToF-CIMS, hereafter as CIMS) (Lopez-Hilfiker et al., 2014). Basic principles and configurations were described in previous field studies (Le Breton et al., 2018a;Le Breton et al., 2018b). Each CIMS operation cycle consisted of background (~2 min), ambient gas (~16 min), a second background (~2 min), and $PM_{2.5}$ desorption measurements (~50 min) (Fig. S5). The background signals were measured by periodically overflowing the inlet with ultrahigh purity N_2 (Laser gases), and background subtractions were performed to minimize potential interference from contamination. The raw signals in counts per second (cps) were normalized by the sum of the reagent ions ($I^- + I{\cdot}H_2O^-$) and multiplied by 10^6. During the field campaign, ~0.3 lpm perfluoropentanoic acid in N_2 was injected into the CIMS (identified as $C_5HF_9O_2I^-$) every 1~2 days for mass calibration. The sensitivities of acetic acid, which was generated from a permeation source (permeation rate of 184.5 ng/min at 40°C), was measured periodically on 2/27, 2/28, 3/5, 3/10, 3/12, and 3/14 to track the instrument stability, which was 0.27 ± 0.05 cps/ppt with a variation of 17.7%.

Calibrations of gaseous species were conducted after the campaign under RH conditions (IH_2O^- to I^- ratio 0.42 ± 0.02) similar to those observed during the field measurement in Delhi (IH_2O^- to I^- ratio 0.40 ± 0.08), with sensitivities of 7.5, 3.6, 0.013, 13.6, and 0.29 cps/ppt for N_2O_5, $ClNO_2$, HCl, chloroacetic acid, and acetic acid, respectively. The sensitivity of acetic acid measured post-campaign (0.29 cps/ppt) agreed well with the on-site calibration result (0.27 cps/ppt), and therefore no additional scaling was applied for the on-site sensitivities of the detected species. Sensitivities for Cl_2 (3.4

cps/ppt), NCl_3 (3.1 cps/ppt), and $NHCl_2$ (0.05 cps/ppt) were estimated using their relative sensitivities to $ClNO_2$ (Chen et al., 2025b). The detection limits were determined as three times the standard deviation of the hourly averaged background signals, which were 0.6 ppt for N_2O_5, 1.6 ppt for $ClNO_2$, 0.6 ppt for Cl_2, 22.6 ppt for $NHCl_2$, 0.3 ppt for NCl_3, 209.1 ppt for HCl, and 2.5 ppt for chloroacetic acid, respectively. For the remaining detected gaseous compounds, mainly oxygenated organics consisting of carbon, hydrogen, and oxygen (abbreviated as CHO) or carbon, hydrogen, oxygen, and nitrogen (abbreviated as CHON), the maximum value of the calibrated sensitivities (chloroacetic acid, 13.6 cps/ppt) was used to derive conservative concentration estimates. For particulate compounds, the calibrated sensitivity of levoglucosan (2.2×10^5 ions/ng) was applied to obtain lower-limit estimates, as the detection of levoglucosan has recently been demonstrated to proceed at the collision limit (Aggarwal et al., 2025).

EDXRF. Ambient $PM_{2.5}$ filter samples were collected for offline Energy Dispersive X-ray Fluorescence (EDXRF; SPECTRO-XEPOS, AMETEK Inc.) analysis. ED-XRF is a sensitive and non-destructive technique which requires negligible sample pre-treatment and has been widely used for measuring elements in ambient particles (Ogrizek et al., 2022;Unga et al., 2025). A total of 83 $PM_{2.5}$ samples were collected at 3 lpm on polytetrafluoroethylene (PTFE) filters (25 mm in diameter of 0.4 μm) via a $PM_{2.5}$ cyclone (Casella Solutions, UK) every 12 hours from 2/22 to 2/28 and every 4 hours from 3/1 to 3/14. We increased the frequency of filter switches by the end of the campaign to capture the variations of Cl element concentrations within a night, i.e., before (19:00~23:00) and post (23:00~3:00) midnight. The mid-point of the measurement period, i.e., 1:00 indicates measurement from 23:00~3:00, 5:00 for 3:00~7:00, 9:00 for 7:00~11:00, 13:00 for 11:00~15:00, 17:00 for 15:00~19:00, and 21:00 for 19:00~23:00, was used as the representative timestamp for each filter sample. Four blank filters (without any air sampling) were collected during the daytime (7:00~19:00) on 3/5 and 3/11, and during nighttime (19:00~7:00) on 3/5 and 3/8. These blank filters underwent the same analytical procedures as the sample filters. The filter samples were directly analyzed by EDXRF without any pretreatment. Each sample was analyzed for approximately 22 minutes. The instrument measured 26 elements, i.e., Al, Si, P, S, Cl, K, Ca, Ti, V, Cr, Mn, Fe, Co, Ni, Cu, Zn, Ga, Ge, As, Se, Br, Sr, Ba, Ti, Pb and Bi, based on their characteristic fluorescence (150 eV to 600 eV). This manuscript reports the blank-subtracted concentrations of K and Cl.

The EDXRF instrument detects the total concentrations of elements in the collected filter samples, while the CIMS detects compounds that evaporate at temperatures up to 200 ºC. Persistent signals of $HCl{\cdot}I^-$ were observed from $PM_{2.5}$ desorption during the CIMS measurement (Fig. S5), likely originating from the thermal decomposition of non-refractory chloride (e.g, NH_4Cl). The trend of chloride measured by CIMS (pCl^--CIMS) largely followed that of the XRF-measured chloride (Cl-XRF) (r = 0.70) (Fig. S6a). Since pCl^--CIMS was not calibrated, it was only used qualitatively to complement the average diurnal variations of Cl-XRF. Cl-XRF was used for further analysis throughout the manuscript.

Supporting measurements. Supporting measurements at IIT Delhi include trace gases O_3 (ECOTECH Serinus 10), NO and NO_2 (ECOTECH Serinus 40), SO_2 (ECOTECH Serinus 50), and CO (ECOTECH Serinus 30) and meteorological parameters (T, RH, wind speed, and wind direction), which were measured by an automated weather station (AWS) (Davis Vantage Pro 2, Davis Instruments Corporation, USA). These concurrent online supporting measurements at IIT Delhi were used for key kinetic parameters calculations, such as $P(NO_3\cdot)$ and $NO_3\cdot$ reactivity, and the analysis of the CIMS data. Hourly $PM_{2.5}$ concentrations and solar radiation data were obtained from the nearest national monitoring station, the R.K. Puram station operated by Delhi Pollution Control Committee (DPCC), which is located approximately 3 km northwest of IIT Delhi. Intercomparison of the trace gases, T, and RH measured at IIT Delhi and R.K. Puram showed overall good agreement (Fig. S6c). The solar radiation was converted to photolysis frequency (j) of NO_2 (j_{NO2}) utilizing the method from Trebs et al (Trebs et al., 2009). The estimated j_{NO2} was then used to derive real-time photolysis frequency of $NO_3\cdot$, O_3 and reactive chlorines (Chen et al., 2025b). Additional details about the field observations are shown in Text S1.

Comparison with the measurements in 2019 (Haslett et al., 2023) was used to investigate the evolution of N_2O_5-$ClNO_2$ chemistry under different chemical regimes (e.g., NO and chloride concentrations) in Delhi. It is noted that throughout the manuscript, "in 2023" and "in 2019" refer to the corresponding field campaigns conducted from 23 February to 14 March in 2023 (this study) and from 11 January to 5 February in 2019 (the previous campaign), respectively.

2.2 Kinetic calculations

N_2O_5-$ClNO_2$ chemistry. Key kinetic parameters were derived to investigate factors controlling the variations of N_2O_5 and $ClNO_2$ and compare with previous studies. The field-constrained uptake parameter, defined as the product ($\gamma_{N_2O_5}\times f_{ClNO_2}$) of the N_2O_5 uptake coefficient ($\gamma_{N_2O_5}$) and $ClNO_2$ yield (f_{ClNO_2}), as is shown in Eq. 1, was calculated hourly using neighboring measurements during the nighttime following Eq. 3b in Mielke et al.(Mielke et al., 2013) (Eq. 1), assuming the local heterogeneous uptake of N_2O_5 was the sole source of the measured $ClNO_2$ and that $ClNO_2$ experienced negligible nocturnal losses.

$$\left[\gamma_{N_2O_5}\times f_{ClNO_2}\right]_{t0} = \frac{[ClNO_2]_{t1}}{\int_{t0}^{t1}\frac{1}{4}\bar{c}S_a[N_2O_5]_{t0}dt} \quad \text{(Eq. 1)}$$

$$\bar{c} = \sqrt{\frac{8kT}{\pi m}} \quad \text{(Eq. 2)}$$

where $\bar{c}$ is the average molecular velocity of N_2O_5, $m\cdot s^{-1}$; T is temperature in Kelvin; k is Boltzmann's constant, 1.38×10^{-23} $m^2\cdot kg\cdot s^{-2}\cdot K^{-1}$; m is the molecular weight of N_2O_5, kg, which is calculated as the molar mass of N_2O_5 ($kg\cdot mol^{-1}$) divided by the Avogadro's number (mol^{-1}); Sa is aerosol surface area,

$m^2 \cdot m^{-3}$, which is not directly measured but inferred from $PM_{2.5}$ data. Based on the linear correlation between $PM_{2.5}$ and Sa observed by Gani et al. (Gani et al., 2020) from February to March 2018, we used $PM_{2.5}$ concentrations from our 2023 campaign to derive the corresponding Sa values (Fig. S6b, r = 0.78). This estimation of Sa using $PM_{2.5}$ has also been employed and validated in other studies (Meidan et al., 2022;Zhang et al., 2025); t0 is the current time point, t1 is the subsequent time point, and dt is the time interval (in seconds) between them.

The theoretical values of the uptake parameter ($\gamma_{N_2O_5} \times f_{ClNO_2}$) range from 0 to 0.1, as the maximum values of $\gamma_{N_2O_5}$ and f_{ClNO_2} are generally below 0.1 and 1, respectively(Tham et al., 2018). However, nocturnal transport, i.e., changes in air masses, can invalidate this method and yield values exceeding 0.1 (sharp increases in $ClNO_2$, occurrence frequency of ~17%) which were discussed separately (Section 3.2).

The production rate ($P(NO_3)$) and reactivity ($R(NO_3)$) of $NO_3\cdot$ were calculated to evaluate N_2O_5 budgets, which are shown in Eq. 3 and Eq. 4, respectively. The $ClNO_2$ production efficiency ($\varepsilon(ClNO_2)$, Eq. 5), indicating the fraction of the total generated $NO_3\cdot$ overnight that is ultimately transformed into $ClNO_2$, was calculated for comparison with previous studies (Eger et al., 2019;Xia et al., 2025). The integration period was set from 20:00 to 04:00 to minimize influences of potential air mass mixing during the day-night and night-day transition periods.

$$P(NO_3) = k_{NO_2+O_3}[NO_2][O_3] \quad \text{(Eq. 3)}$$

$$\mathrm{R}(NO_3) = k_{NO+NO_3}[NO] + j_{NO_3} + k_{hete}[NO_2]K_{eq} + \sum k_i[VOC_i] \quad \text{(Eq. 4)}$$

$$\varepsilon(ClNO_2) = \frac{[ClNO_2]_{max}}{\int_{20:00}^{04:00} P(NO_3)} \quad \text{(Eq. 5)}$$

$$\gamma(\mathrm{N_2O_5}) = RH \times 5.2 \times 10^{-4} \quad (RH \leqslant 57\%) \text{ (Eq. 6.1)}$$

$$\gamma(\mathrm{N_2O_5}) = 0.03 \quad (RH > 57\%) \quad \text{(Eq. 6.2)}$$

where $k_{NO_2+O_3} = 1.2 \times 10^{-1} \times \exp(-2450/T)$ $cm^3 \cdot molec^{-1} \cdot s^{-1}$ and $k_{NO+NO_3} = 1.8 \times 10^{-11} \times \exp(110/T)$ $cm^3 \cdot molec^{-1} \cdot s^{-1}$ (Burkholder et al., 2020); j_{NO3} is the photolysis frequency of $NO_3\cdot$ and is retrieved from the Tropospheric Ultraviolet and Visible (TUV) radiation model and scaled with the field constrained j as discussed previously; k_{hete} is the first-order heterogeneous loss rate coefficient of N_2O_5, where $k_{he} = \frac{\bar{c}\gamma_{N_2O_5}Sa}{4}$; $\gamma_{N_2O_5}$ was parametrized using Eq. 6 according to the experimental measurements of N_2O_5 uptake on aqueous organic aerosols (Evans and Jacob, 2005;Thornton et al., 2003). This parameterization method was supported by the consistency between the simulated nocturnal $ClNO_2$ variations using the RH-parameterized $\gamma_{N_2O_5}$ and the observed $ClNO_2$ levels, as detailed in Text S2; K_{eq} is the equilibrium constant between $NO_3\cdot$, NO_2, and N_2O_5, where $K_{eq} = 5.5 \times 10^{-2} \times \exp(10724/T)$ (Wängberg et al., 1997). $\sum k_i[VOC_i]$ is the sum of $NO_3\cdot$ reactivity with different VOCs and we applied the same value of 0.081 s^{-1} in 2023 as in 2019 (Haslett et al., 2023)

due to the lack of concurrent VOCs measurements in 2023. As shown in Fig. S7a and Table S2, the campaign-averaged NO_3· reactivity to NO in 2023 is ~15.6 s^{-1}, which is approximately 2 orders of magnitude higher than the reactivity to VOCs and the heterogeneous loss of NO_3· from N_2O_5 uptake (0.091 s^{-1}). Limited field measurements in Mohali (Meidan et al., 2022) and Delhi (Wang et al., 2020;Mishra et al., 2024) showed that the total VOC concentrations exhibit inter-annual and seasonal variations ranging from a factor of less than two to approximately four. In this context, though we don't expect that the lack of concurrent VOCs observations would significantly influence the estimated total NO_3· reactivity during the 2023 campaign, which is likely dominated by reactions with NO, it should be emphasized that the exact value of NO_3· reactivity towards VOCs may deviate from the assumed value (0.081 s^{-1} on average). This uncertainty stems from the temporal and spatial changes in VOC speciation, concentration and reactivity. Long-term and dense VOCs measurements will help to better quantify NO_3· reactivity in Delhi.

Production rates of Cl· and OH· radicals. The Cl· production rate (P(Cl·)) is calculated according to Eq. 7. For the 2023 campaign, we calculated P(Cl·) both from $ClNO_2$ photolysis and from all the detected photolabile reactive chlorines. A direct comparison between 2019 and 2023 was conducted using P(Cl·) from $ClNO_2$ photolysis. In 2019, only $ClNO_2$ photolysis was considered as a source of Cl·, since mixing ratios of other reactive chlorines were not reported in the previous study (Haslett et al., 2023). Additionally, we estimated a lower-limit OH· production rate (P(OH·)) in Delhi from the photolysis of O_3 in the presence of water vapor (Eq. 8) (Dunlea and Ravishankara, 2004).

$$P(Cl) = j_{ClNO_2}[ClNO_2] + 2 \times j_{Cl_2}[Cl_2] + j_{NCl_3}[NCl_3] + j_{NHCl_2}[NHCl_2] \quad \text{(Eq. 7)}$$

$$P(OH) = \frac{2 \times j_{O^1D}[O_3] + k_{H_2O}[H_2O]}{k_{H_2O}[H_2O] + k_{N_2}[N_2] + k_{O_2}[O_2]} \quad \text{(Eq. 8)}$$

where j_{O^1D} is the photolysis frequency of O_3, $k_{H_2O} = 1.6 \times 10^{-10} \times \exp(60/T)$, $k_{N_2} = 2.2 \times 10^{-11} \times \exp(110/T)$, and $k_{O_2} = 3.3 \times 10^{-11} \times \exp(55/T)$ (Burkholder et al., 2020).

3 RESULTS AND DISCUSSION

3.1 Characteristics of N_2O_5 and $ClNO_2$ variations

We observed pronounced nocturnal enrichment of N_2O_5 and $ClNO_2$ in 2023 (Fig. 1a, b). N_2O_5 and $ClNO_2$ up to 566 and 1340 ppt were measured during the nighttime, with mixing ratios frequently exceeding 10 and 100 ppt, respectively (Fig. S8). Overall, the nighttime N_2O_5 and $ClNO_2$ mixing ratios in 2023, with an average of 13.1 ppt and 80.1 ppt, respectively, are significantly (Mann-Whitney test, p<0.01) higher than those measured in 2019 (4.5 and 36.3 ppt, respectively) (Fig. 1a, b).

As shown in Table S3, the maximum N_2O_5 mixing ratio in Delhi is a third to half of those observed in urban areas of the United States (Thornton et al., 2010;Osthoff et al., 2008) and England (Bannan et al., 2015), and approximately an order of magnitude lower than those measured in aged air plumes from industrial regions in China (Chen et al., 2023;Wang et al., 2016;Ye et al., 2021). By contrast, the peak $ClNO_2$ level in Delhi is much higher than those reported in urban regions of the North America

(Thornton et al., 2010;McNamara et al., 2020;Wang et al., 2023a) and Europe (Bannan et al., 2015;Phillips et al., 2012;Priestley et al., 2018), and similar to or 1~2 times lower than those observed in the North China Plain (Tham et al., 2016;Xia et al., 2021;Peng et al., 2021;Chen et al., 2025a). The observed pattern of low N_2O_5 and high $ClNO_2$ indicates efficient conversion of N_2O_5 to $ClNO_2$ in Delhi.

We further examined N_2O_5 and $ClNO_2$ variations every night and classified them into the enhanced and non-enhanced cases (Fig. S9 and Fig. S10). Among the enhanced cases, elevated N_2O_5 mixing ratios exceeding 10 ppt were characterized by both relatively low NO (median 3 ppb) and particulate Cl (median 0.7 μg/m^3) concentrations, and appreciable $ClNO_2$ levels larger than 100 ppt were observed under moderate NO (median 7 ppb) and high particulate Cl (median 3.3 μg/m^3) conditions (Fig. S9). No notable N_2O_5 or $ClNO_2$ mixing ratios were measured among the non-enhanced cases when NO levels were relatively high (median 31 ppb) (Fig. S10). The occurrence frequency of the enhanced cases (11 out of total 19 nights) is higher than the non-enhanced (8 nights) cases.

The measured N_2O_5 generally presents transient, spike-like patterns in 2023 (Fig. S8), peaking around the early evening (18:00~20:00) when both NO and particulate Cl are relatively low, and tapering off as the night proceeds (Fig. 1a, c-d). In comparison, the $ClNO_2$ mixing ratio gradually built up after midnight with the increase of particulate Cl, reaching the highest level during the early morning hours (06:00~08:00, Fig. 1b, d). Overall, the nocturnal N_2O_5 mixing ratio shows a significant negative dependency (r = -0.64, p<0.01) on the NO concentration (Fig. 2a), and high $ClNO_2$ levels were accompanied by abundant chloride (Fig. S11a), indicating the critical roles of NO and chloride in controlling N_2O_5 and $ClNO_2$ formation in Delhi.

The nocturnal mean $ClNO_2$ production efficiency ($\varepsilon(ClNO_2)$) also increases from 3.0% in 2019 to 4.3% in 2023, which is comparable to the values reported in marine and coastal areas(Eger et al., 2019;Xia et al., 2025). In addition, the diurnal profile of N_2O_5 in 2023 was inverted compared to 2019, with higher levels in the early evening rather than during the daytime (Fig. 1a). Consistently, distinct diurnal variations of N_2O_5 were also observed under relatively low- and high-NO conditions in 2023 (Fig. S12). The emerging early evening peak of N_2O_5 leads to a new N_2O_5-driven $ClNO_2$ enhancement pattern in 2023 (the dashed linear fitting line in Fig. 1e), characterized by a strong positive correlation (r = 0.93) between N_2O_5 and $ClNO_2$ under conditions of elevated N_2O_5 (10~400 ppt) and limited chloride (0.1~3.4 μg/m^3). This pattern resembles those observed in other continental air masses (Thornton et al., 2010;Bannan et al., 2015;Zhou et al., 2018), while the $ClNO_2$ to N_2O_5 ratios are slightly higher in Delhi, ranging from 0.3 to 3.2, with an average of 1.2. Notably, despite the substantial decline in particulate Cl from 2019 (20.8 μg/m^3) to 2023 (4.7 μg/m^3), the higher $ClNO_2$ levels in 2023 indicate that the promoting effect of elevated N_2O_5 potentially outcompetes the limiting impact of reduced chloride. Additionally, the estimated $ClNO_2$ yield is around unity in Delhi (Fig. S13a).

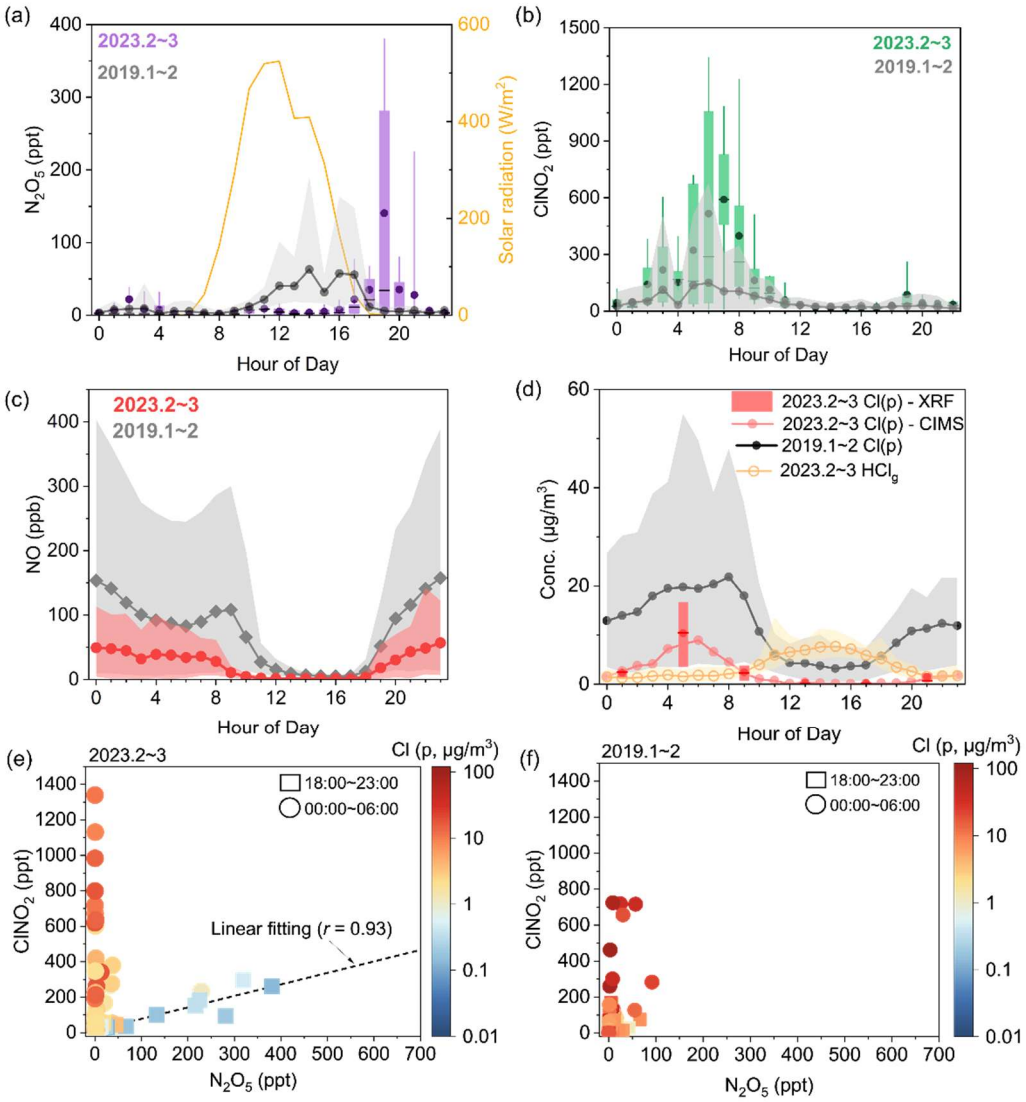

Fig. 1 Field characterization of N_2O_5 and $ClNO_2$ in Delhi. Campaign-averaged diurnal variations of (a) N_2O_5, (b) $ClNO_2$, (c) NO, and (d) particulate Cl and gaseous HCl. Scatter plots of N_2O_5 versus $ClNO_2$ mixing ratios in (e) 2023 and (f) 2019, color-coded by the particulate Cl concentrations. The observation (Haslett et al., 2023) in 2019 is included for comparison, where the gaseous HCl measurements are not available. The right axis in (a) indicates solar radiation during the campaign in 2023. The exact sunrise (07:07~07:15) time in 2019 is about 30 min later than that in 2023 (06:55~06:32), while the sunset time in 2019 (17:24~18:03) is about 30 min earlier according to the records from timeanddate website. Gaseous HCl and particulate Cl measured by CIMS are also shown in (d). The upper and lower edge of the box and whisker in (a), (b) and (d) represent the 25th and 75th, and 10th and 90th percentiles, respectively. The dots and squares denote mean values and the lines inside the boxes indicate median levels. The shaded area in (a)-(d) indicates the 10th and 90th percentile range.

3.2 Influencing factors of N_2O_5-$ClNO_2$ chemistry

Decreased NO concentrations in 2023 relative to 2019 reduce NO_3· losses to reactions with NO, resulting in elevated nocturnal N_2O_5 levels. The reaction with NO dominated NO_3· losses both in 2019 and 2023 (~99%, Table S2 and Fig. S7a), contributing to the low abundances and short-lived occurrences of N_2O_5 in Delhi (Haslett et al., 2023). The strong anti-correlation between nocturnal N_2O_5 and NO persists in 2023, where the N_2O_5 mixing ratios overlap with those in 2019 when NO concentrations are within the same range (approximately 2–100 ppb) (Fig. 2a). However, in 2023, the frequency of relatively low-NO conditions (<2 ppb) rose from 0 to 8% and extreme NO levels (>100 ppb) nearly disappeared, indicating that NO titration in suppressing N_2O_5 production has diminished (Fig. 2a). With the decline in NO concentrations from 2019 (nighttime averages 124 ± 25 ppb) to 2023 (44 ± 9 ppb) (Fig. 1c), the nighttime average NO_3· reactivity towards NO dropped by ~66% from 83.7 s^{-1} to 28.4 s^{-1}, extending NO_3· lifetimes approximately two folds during the nighttime in 2023 (0.04 s). The reduced NO_3· losses to NO increased the availability of NO_3· for reacting with NO_2, thereby enhancing N_2O_5 production. Additionally, no significant correlation between chloride and $ClNO_2$ was observed in 2019, likely because the chloride increases were accompanied by a substantial elevation in NO, which suppressed N_2O_5 formation (Fig. S11b).

Higher NO_3· production rates ($P(NO_3)$) enhance N_2O_5 formation. Due to the increases in nocturnal O_3 levels (from 3.5 to 6.8 ppb) and the reaction rate constant between NO_2 and O_3 (from 2.36×10^{-17} to 2.93×10^{-17} $cm^3\cdot molec^{-1}\cdot s^{-1}$), the average nocturnal $P(NO_3)$ in 2023 almost doubled (0.75 ppb h^{-1}) compared to 2019 (0.41 ppb h^{-1}) (Fig. 2b). The observed ($P(NO_3)$) in Delhi 2023 exceeds those reported in the United States (Wang et al., 2023b;Noxon et al., 1980) and Europe (Ljungström and Hallquist, 1996;Wang et al., 2023b), and 1~2 times lower than those observed in China (Wang et al., 2024;Yan et al., 2021;Chen et al., 2023). Consistently, N_2O_5 mixing ratios in 2023 peak after sunset around 18:00~19:00 (Fig. 1a), coinciding with the period of elevated $P(NO_3)$ (Fig. 2b) and relatively low NO levels (Fig. 1c). Other factors, such as the decreased aerosol surface area (2637 ± 152 and 1411 ± 162 $\mu m^2/cm^3$ in 2019 and 2023, respectively) results in reduced first-order heterogenous loss rate coefficient of N_2O_5 (k_{hete}) from 0.74 ± 0.09 s^{-1} in 2019 to 0.14 ± 0.02 s^{-1} in 2023, which also contributes to the elevated nocturnal N_2O_5 mixing ratios observed in 2023. Overall, the enhanced NO_3· production and reduced losses to NO led to elevated NO_3· and N_2O_5 levels in 2023, aligning with the higher estimated steady-state NO_3· mixing ratios (0.25 ppt vs. 0.03 ppt in 2019) (Fig. S7b).

As is shown in Fig. S1c, NO_x emissions in Delhi almost doubled in recent years, mainly driven by the increase in the number of vehicles (Beig, 2010, 2018;Sahu et al., 2023). The observed decrease in NO concentrations during the 2023 campaign is therefore not driven by the changes in emissions. Notably, the 2019 and 2023 measurements were conducted in different seasons, i.e., January to early February (winter) in 2019 and late February to mid-March (early spring) in 2023. As is shown in Fig. S14, elevated O_3 concentrations were observed in spring compared to winter, which facilitates the

removal and decrease of NO and P(NO_3). Overall, the seasonal variability in NO concentrations is the main driver of the differences in NO and P(NO_3) observed between the two campaigns.

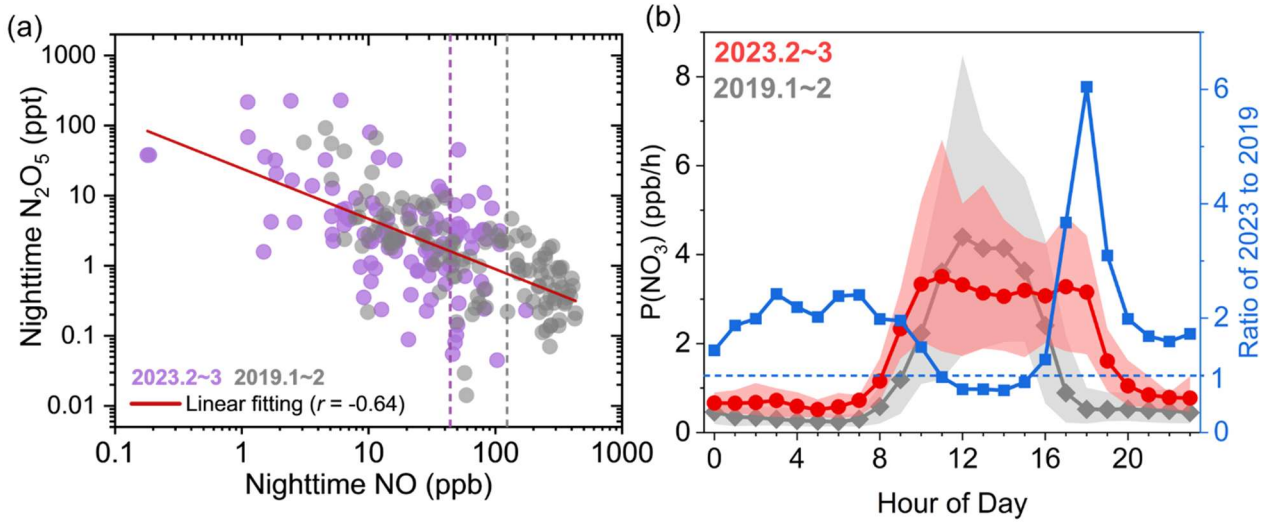

Fig. 2 Factors contributing to nocturnal N_2O_5 enhancement. (a) Scatter plot of nighttime NO versus N_2O_5. Nighttime is defined as the period from 20:00 to 04:00, excluding the transition period between day and night when the air mass was unstable. The purple and grey dashed lines indicate the average NO concentrations during the 2023 and 2019 campaign, respectively. (b) Campaign-averaged diurnal variations of P(NO_3) in 2023 and 2019, respectively. The right axis in (b) displays the 2023-to-2019 ratio of P(NO_3). The dots and squares denote mean values and the shaded area indicates the 10^{th} and 90^{th} percentile range.

High chloride concentrations promote N_2O_5 uptake and $ClNO_2$ production in Delhi. The field-derived uptake parameter ($\gamma \times f$) in Delhi is similar to those observed in marine air (~0.02 on average)[11] and several times to an order of magnitude higher than those reported in other continental regions (6×10^{-4}~8×10^{-3}) (Xia et al., 2021;Tham et al., 2018;Xia et al., 2020;Mielke et al., 2013). As is shown in Fig. 3a, this parameter increases with the chloride level in Delhi, reflecting the combined effects of chloride in promoting N_2O_5 uptake and $ClNO_2$ yield observed in prior laboratory studies (Bertram and Thornton, 2009;Jahl et al., 2021). By contrast, despite comparable high chloride was observed in Wangdu (Xia et al., 2021) (upper triangle in Fig. 3b), both the uptake parameter (~6×10^{-4} on average) and the nocturnal $ClNO_2$ level (typically <50 ppt) are significantly lower than those measured in Delhi. This is likely due to the lower ambient water content (~0.4%) compared to Delhi (~1.5%), which limits aerosol liquid water content and thereby suppresses N_2O_5 hydrolysis on particles (Xia et al., 2021;Tham et al., 2018).

The high chloride in Delhi is largely in the form of semi-volatile NH_4Cl, originating from gas to particle partitioning. We observed a concurrent late-evening enrichment of non-refractory chloride measured by CIMS and Cl element measured by XRF (Fig. 1d), indicating the semi-volatile nature of

particulate Cl (i.e., NH_4Cl) in Delhi. Additionally, direct measurements of both HCl and particulate Cl enabled us to examine the gas–particle partitioning behavior of Cl. As shown in Fig. 3b, the particle-phase Cl fraction amounted to up to 89% on average at 6:00 whereas it remained below 20% in the afternoon (12:00-18:00). This diurnal variation is attributed to lower temperatures (15-25 °C) and higher RH (56-92%) in the early morning hours, which favored the co-condensation of HCl and water vapor into particles as NH_4Cl under the NH_3-rich conditions commonly found in Delhi (Acharja et al., 2023;Gunthe et al., 2021). A recent study suggests that increasing RH promotes the migration of chloride from the particle bulk phase to the gas-particle interface (Fauré et al., 2024). This phenomenon helps explain the observed post-midnight accumulation of $ClNO_2$ and consistently low N_2O_5 levels in Delhi, which are attributed to enhanced heterogeneous conversion of N_2O_5 to $ClNO_2$ on aerosol surfaces. The observed thermodynamically-driven partitioning behavior of Cl agrees with previous model simulations (Gunthe et al., 2021;Chen et al., 2022b).

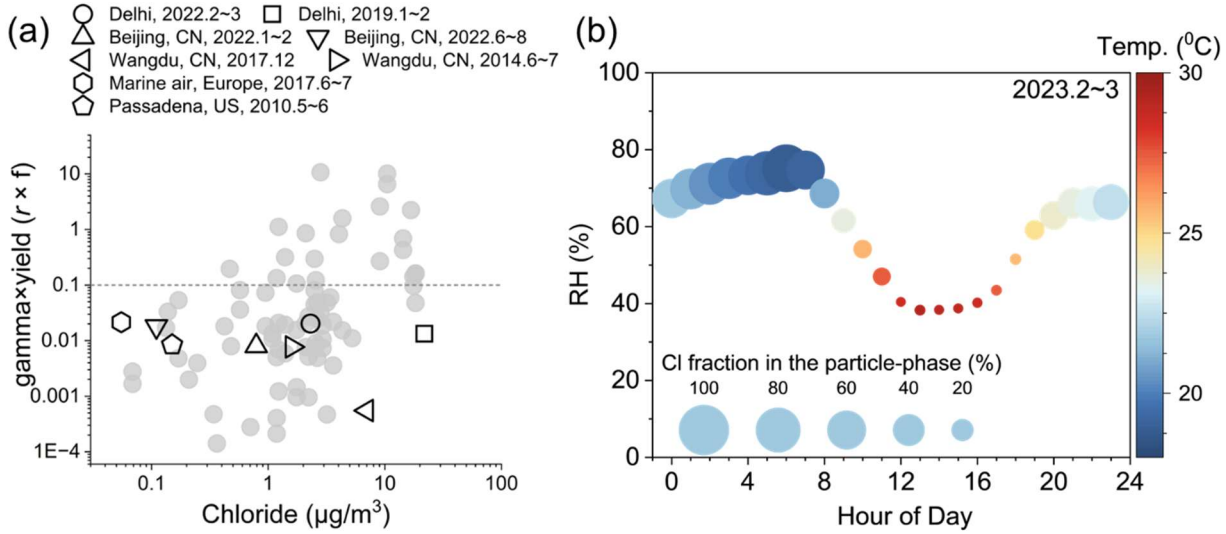

Fig. 3 Factors contributing to nocturnal $ClNO_2$ enhancement in Delhi. (a) Dependence of the field-observed uptake parameter ($\gamma \times f$) on particulate Cl concentrations in 2023. The campaign-average value for 2023 (excluding unusually high values of $\gamma \times f > 0.1$) is shown as an open circle. The values derived from previous observations in Delhi 2019 (Haslett et al., 2023), Beijing (Chen et al., 2025b), Wangdu (Xia et al., 2021;Tham et al., 2018), Pasadena (Mielke et al., 2013), and marine air in Europe (Eger et al., 2019) are shown as different markers. The reference line of $\gamma \times f$ equals to 0.1 is also plotted. (b) Campaign-averaged diurnal variation of RH in 2023, color-coded by ambient temperature. The size of the datapoints is proportional to the observed Cl fraction in the particle-phase, which is calculated as $Cl_p/(Cl_p + HCl_g)$.

$ClNO_2$ levels in Delhi were influenced by the transport of $ClNO_2$-laden biomass burning plumes from upwind regions, and vertical intrusion initiated by the breakup of the residual layer during the early morning (6:00~8:00). We observed some cases with unusually high $\gamma \times f$ values exceeding 0.1, implying additional $ClNO_2$ sources beyond the local N_2O_5 uptake. Most of the high values were found

during episodes of easterly (50~130°) winds with elevated particulate Cl concentrations (Fig. 4a), when the air masses passed over biomass-burning hotspots (Fig. S15). This suggests substantial $ClNO_2$ production on high chloride containing biomass burning aerosols, as observed in previous laboratory experiments (Ahern et al., 2018;Jahl et al., 2021). A typical case is shown in Fig. S16**,** where $ClNO_2$ abruptly increases concurrently with the sharp rise in particulate Cl, biomass-burning tracers (K and HCN), and easterly wind speeds. Additionally, a continued rise in $ClNO_2$ was observed after sunrise (6:00~8:00; Fig. 1b and Fig. S16), likely due to the downward mixing of $ClNO_2$-rich air masses aloft, as reported in previous studies (Tham et al., 2016;Haslett et al., 2023).

Delhi is an inland city located roughly 1,000 kilometers away from the nearest coastlines. Significant chlorine emissions from natural sea salt aerosols are not expected. The high chloride levels observed in Delhi point to intense chlorine emissions from anthropogenic sources. The nighttime Cl strongly correlates with K ($r = 0.82$) and HCN ($r = 0.73$) (Fig. 4b-c and Fig. S17), indicating significant Cl emissions from biomass burning in Delhi. The ambient nighttime Cl to K ratio (1.6 ± 0.8) in Delhi is about three-fold higher (0.4 ± 0.2) than those measured from biomass/biofuel emission sources (Table S4), indicating additional sources of Cl potentially from plastic-contained garbage burning, industrial processes, and coal combustion (Gunthe et al., 2021). Consistently, we observed a moderate correlation between Cl and and the coal combustion tracer SO_2 (r = 0.51). In contrast, the poor correlation of Cl with NO (r = -0.30) and CO (r = -0.08) indicated limited contributions from vehicle exhaust, consistent with their low Cl emission factors (Table S4).

Since the above discussions are built on two short-term campaigns, we further assess the prevalence of N_2O_5 and $ClNO_2$ production in Delhi based on the long-term distributions of the identified influencing factors, i.e., NO, $P(NO_3)$, and chloride (Fig. S3). The occurrence distribution of nighttime NO and $P(NO_3)$ during the 2023 campaign largely overlapped with the conditions commonly occurred in Delhi (Fig. S3a-b), indicating comparable N_2O_5 production potential throughout the years in Delhi. In addition, the occurrence frequency distribution of chloride in 2023 campaign is comparable to that observed from January to April of 2022 and much higher than those reported from May to September (Fig. S3c). The seasonal variation of chloride reflects the temperature-driven evaporation of semi-volatile NH_4Cl as discussed previously. Given the critical role of chloride in promoting N_2O_5 uptake and driving $ClNO_2$ production in Delhi, these results suggest that elevated nighttime N_2O_5 and $ClNO_2$ levels are most likely observed during the warm and cold seasons, respectively, in Delhi.

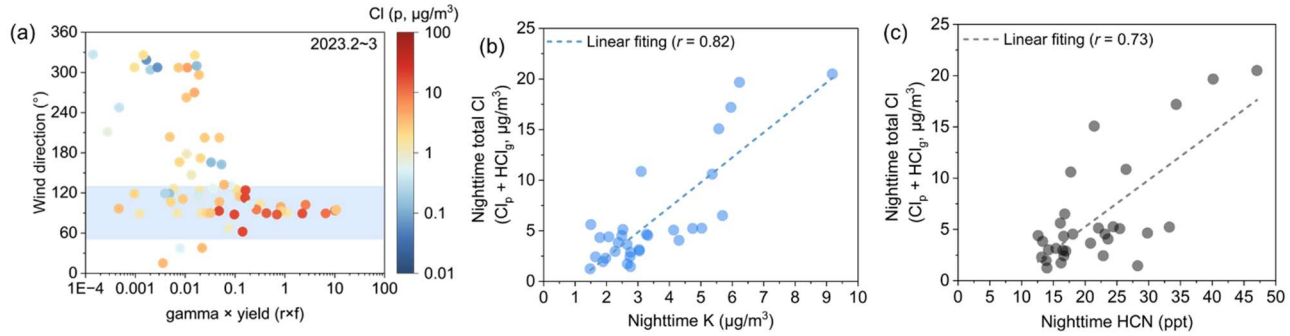

Fig. 4 Potential sources of chlorine in Delhi. (a) Scatter plot of uptake parameter ($\gamma \times f$) and wind direction color-coded by particulate Cl concentrations. The shaded area in (a) indicates the region with wind direction ranging from 50° to 130°. Correlation of nocturnal total Cl (sum of Cl_p and HCl_g) with (b) particulate K and (c) gaseous HCN. The reported HCN mixing ratio can be considered a lower-limit estimate (see Methods 2.1).

3.3 Impacts on atmospheric radical production and VOCs oxidation

Enhanced N_2O_5-$ClNO_2$ chemistry at lower NO levels emphasizes the important roles of Cl· and NO_3· in initiating the oxidation of VOCs in Delhi. The average daytime P(Cl·) from $ClNO_2$ photolysis in 2023 (0.035 ppb/h) is about approximately twice that observed in 2019 (0.015 ppb/h). The maximum daytime-averaged P(Cl·) (0.24 ppb/h) from the photolysis of all the detected Cl· precursors (Cl_2, $ClNO_2$, $NHCl_2$, and NCl_3) is up to an order of magnitude higher than values reported for the urban inland areas of Europe and North America (0.02~0.07 ppb/h) (Priestley et al., 2018;McNamara et al., 2020;Faxon et al., 2015), and remains several times lower than those observed during the pollution episodes in China (0.5~1.1 ppb/h) (Chen et al., 2023;Tham et al., 2016;Liu et al., 2017). $ClNO_2$ photolysis dominates the production of Cl· around the sunrise hours (7:00~8:00) when the $P(Cl\cdot)_{total}$ to P(OH) ratio (42 on average) was also the highest (Fig. 5a), suggesting non-negligible Cl-initiated oxidation of VOCs under these conditions in Delhi.

Consistently, we observed specific gaseous organic oxidation products indicative of the prevalence of chlorine chemistry (Fig. 5b). We identified organochlorinated species, i.e., $C_2H_3O_2Cl$ and $C_3H_5O_2Cl$ (presumably chloroacetic acid and chloropropionic acid), which were previously measured in chamber experiments from Cl· reacting with ethylbenzene (Jahn et al., 2024) and isoprene (Wang et al., 2022) and used as markers for the occurrence of chlorine chemistry in field studies (Priestley et al., 2018;Li et al., 2025). The daytime concentration fraction of $C_2H_3O_2Cl$ in the total measured gaseous organics increases from ~0.9% in 2019 to ~1.8% in 2023. Additionally, the daytime average peak mixing ratio of $C_2H_3O_2Cl$ (~100 ppt) in 2023 is about 5~30 times higher than those measured in Hong Kong (12~20 ppt) (Li et al., 2025) and Manchester (~3 ppt) (Priestley et al., 2018), indicating significant $C_2H_3ClO_2$ production in Delhi. We also identified a series of hydroxynitrates (HN) homologues, i.e., $C_8H_{17}O_4N$, $C_{10}H_{21}O_4N$, and $C_{12}H_{25}O_4N$, which were potentially early-generation products from the chlorine-initiated oxidation of $C_{8,10,12}$-alkanes under high NO_x conditions

(Wang and Hildebrandt Ruiz, 2018). Here their sharp increase in the early morning hours (7:00~8:00) when Cl· was likely the dominant atmospheric oxidant (Fig. 5a-b), together with the positive correlations between these HN and the product of P(Cl) and NO ($r_{7:00\sim8:00}$= 0.59, Fig. 5e), underscores the Cl· initiated alkane oxidation in the presence of NO as an important source of HN in Delhi. It is noted that these HN can also be formed via OH-initiated oxidation processes (Lim and Ziemann, 2009), but would then likely peak later in the day when OH concentrations are higher. Here, a quantitative comparison between the Cl- and OH-initiated reaction pathways is missing in current study due to the lack of VOCs precursor measurements and warrants further investigation.

The NO_3-initiated nocturnal oxidation of VOCs was strengthened during the 2023 campaign. The fraction of nitrogen-containing organics (CHON) in the total measured gaseous oxygenated organic compounds in 2023 (~46%) was similar to that observed in 2019 (42%). However, the diurnal pattern of the CHON fraction was inversed, exhibiting a moderate increase (~9%) during the nighttime (Fig. 5c), which resembles those found in other locations (Ye et al., 2021;Huang et al., 2019), indicating enhanced nocturnal NO_3-driven organic oxidation in 2023. We further identified the nighttime gaseous organic species with the criteria of average nighttime (20:00~04:00) to daytime (7:00~16:00) mixing ratio larger than 1. Most of the nighttime species are nitrogen-containing compounds, primarily including $C_{4,5,6}H_{3,5,7}O_5N$ and $C_{10}H_{17}O_{4,5}N$ (Fig. 5f), which are typical first-generation oxidation products from NO_3-induced oxidation of heterocyclics (i.e., furan, methylfuran, and dimethylfuran) (Chen et al., 2022a;Joo et al., 2019;Jiang et al., 2020) and monoterpenes (Jenks et al., 2023;Ayres et al., 2015), respectively. These oxidation products exhibited strong intra-group correlations ($r_{20:00\sim4:00}$ = 0.71 to 0.77), whereas the correlations between the $C_{4,5,6}H_{3,5,7}O_5N$ and $C_{10}H_{17}O_{4\text{-}5}N$ groups were weak ($r_{20:00\sim04:00}$< 0.2), confirming their production from distinct precursors. Moreover, their low correlations with CO and NO ($r_{20:00\sim4:00}$ < 0.4) largely exclude direct combustion emissions as the dominant source. Notably, observations of furan-derived NO_3· oxidation products have currently been limited to laboratory studies (Chen et al., 2022a;Joo et al., 2019;Jiang et al., 2020). Our findings offer direct field evidence of NO_3-initiated furan oxidation in the atmosphere.

Another prominent nighttime compound potentially associated with NO_3· induced oxidation is $C_5H_{11}NO_5$ (Fig. 5f), which exhibited the largest nocturnal enhancement among all the observed species, increasing by a factor of 3.6. $C_5H_{11}NO_5$ correlates well with $C_{10}H_{17}O_5N$ ($r_{20:00\sim4:00}$ = 0.71) and shows a marked increase between 18:00 and 19:00 (Fig. 5d), coinciding with the peak of the estimated NO_3· levels (~2.3 ppt) (Fig. S7b). It is thus likely a co-product from the reaction of NO_3· with monoterpenes. However, this compound has not been reported from any NO_3·-initiated oxidation processes (Jenks et al., 2023;Ayres et al., 2015;Xu et al., 2025). Further investigation is required to elucidate the formation mechanisms of $C_5H_{11}NO_5$ in Delhi's atmosphere.

In addition to the specific organic products discussed above, the overall oxidation state of the measured organic aerosols (OA) is elevated in 2023 compared to 2019. The bulk oxygen-to-carbon

(O/C) ratio of OA (0.76 on average) was higher than the value (0.66) reported in the 2019 campaign (Huang et al., 2024), indicating an increased contribution from more oxidized or aged secondary organic aerosols (SOA) (Jimenez et al., 2009). A clear negative dependence of the O/C ratio on NO was observed at night when NO exceeded about 10 ppb (Fig. S18), agreeing with the suppression effect of NO on organic oxidation by increasing the competitive RO_2+NO channel under the radical-limited regime commonly found in Delhi (Nelson et al., 2021;Kenagy et al., 2024). Taken together, the characteristics of the bulk organics provide additional field evidence for the enhanced atmospheric organics oxidation in 2023.

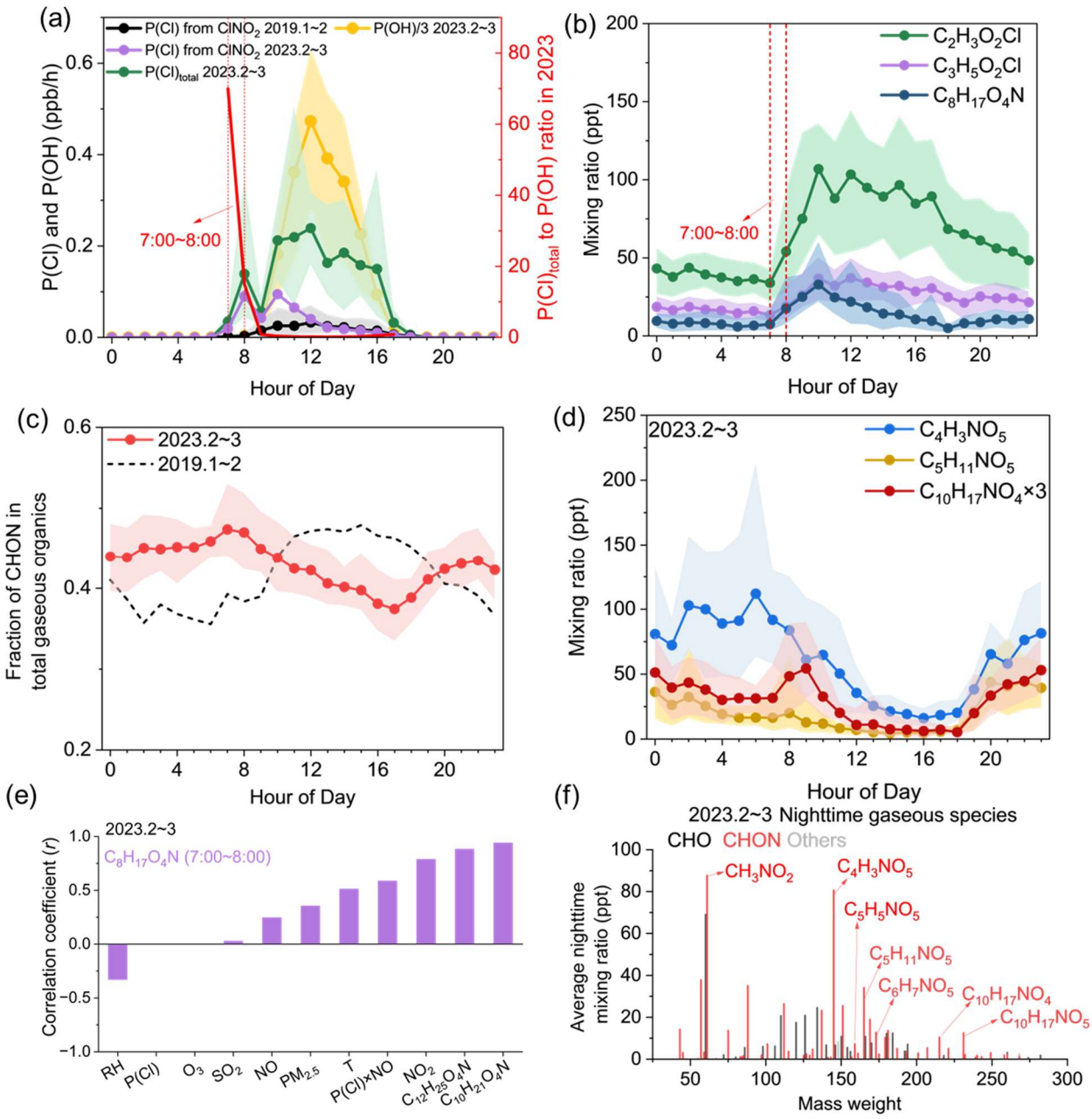

Fig. 5 Enhanced daytime Cl· and nocturnal NO_3· initiated oxidation of organics in Delhi. (a) P(Cl) in 2023 and 2019, and P(OH) from the photolysis of O_3 in 2023. The $P(Cl)_{total}$ 2023 includes

Cl· production from the sum of $ClNO_2$, Cl_2, $NHCl_2$, and NCl_3 photolysis. The $P(Cl)_{total}$ to P(OH) ratio in 2023 is shown in the right axis. The value of P(OH) is divided by a factor of 3 to place it on the same scale as P(Cl). Average diurnal variations of tracer compounds indicating (b) Cl· and (d) NO_3· initiated oxidation, respectively. (c) Comparison of the diurnal variations of CHON compounds fraction in total detected gaseous organics in 2019 and 2023. (e) Correlation coefficients, using observations between 7:00 and 8:00 of $C_8H_{17}NO_4$ with $P(Cl)_{total}$, meteorological parameters, trace gases, and related homologue species. (f) Molecular composition and average nighttime mixing ratios for the nighttime gaseous species. The shaded area in (a-d) indicates the 10th and 90th percentiles and the dots denote mean values.

4 CONCLUSIONS

This study characterized N_2O_5-$ClNO_2$ chemistry in Delhi (Fig. 6). We observed a clear dependency on available nocturnal NO that high NO suppresses N_2O_5 production and reduces the formation of $ClNO_2$ while decreased NO promotes nocturnal N_2O_5-$ClNO_2$ chemistry. The former pattern is consistent with the previously reported significant NO suppression in 2019 (Haslett et al., 2023). With moderate NO in 2023, substantial $ClNO_2$ is produced after midnight hours in Delhi, which is driven by the elevated RH and chloride levels that promote efficient conversion of N_2O_5 to $ClNO_2$. The abundance of chloride strongly correlates with the biomass burning tracers, indicating emissions from biomass burning as an important source of Cl in Delhi. The increased $ClNO_2$ levels at lower nocturnal NO conditions implies that the atmospheric oxidation of organics is amplified both during the nighttime (via NO_3· pathways) and daytime (via Cl· pathways) in Delhi.

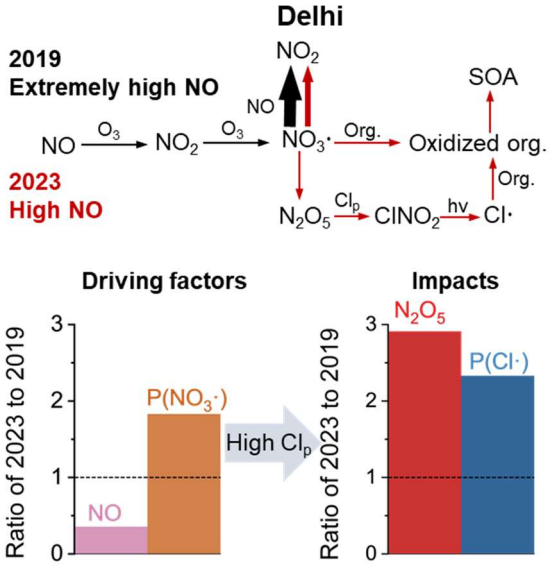

Fig. 6 Amplified N_2O_5 and $ClNO_2$ production and impacts on secondary organic aerosol formation in Delhi. A schematic comparing N_2O_5-$ClNO_2$ chemistry between the 2019 and 2023 campaigns. Red arrows indicate reactions that are largely enhanced during the 2023 campaign.

The differing behaviors of N_2O_5 and $ClNO_2$ depending on the levels of nocturnal NO emphasize the need of continuous monitoring of air pollutants in Delhi, which is essential to understand the evolution of emission sources and atmospheric chemical processes. The complexity of the air pollution situation in Delhi has been further scrutinized where we noted that as chloride levels declined, nitrate has become the leading inorganic component since late 2019 (Fig. S2a-b) and plays an increasingly important role in exacerbating Delhi's $PM_{2.5}$ pollution (Fig. S2c). Thus, future studies should pay attention to elucidating the dominant production pathways of nitrate in Delhi, especially the contribution from N_2O_5 heterogeneous hydrolysis (Wang et al., 2017;Yan et al., 2023).

The present study suggests that NO_x emission control may intensify atmospheric oxidation of organics and secondary organic aerosol (SOA) formation in Delhi, whereas concurrent chlorine emission regulations may help mitigate the associated negative impacts. Previous studies have revealed the critical role chloride has in exacerbating haze formation in Delhi by enhancing aerosol liquid water content (ALWC) (Chen et al., 2022b;Gunthe et al., 2021), while our study implies that, with the decrease in NO concentrations, chloride can also be readily activated into photolabile gases, contributing to the formation of secondary pollutant, e.g., SOA, through generating radicals and advancing atmospheric organics oxidation. An updated chlorine emission inventory combined with modelling studies is necessary to quantitatively evaluate the contribution of chlorine chemistry to $PM_{2.5}$ formation under different NO_x conditions and inform targeted emission control strategies. Finally, the interplay between nitrogen and halogen chemistry in India warrants continued investigation in the context of ongoing industrialization, vehicle electrification, and a changing climate.

Supporting Information

Text S1 to S2, Table S1 to S4 and Fig. S1 to S20

Acknowledgments

We acknowledge financial support from National Natural Science Foundation of China (grant no. 22188102), Tsinghua Scholarship for Overseas Graduate Studies (contract no. 2023012), Swedish Research Council (grant no. 2023-045209), the Swedish Research Council for Sustainable Development (grant no. 2020-02009 and 2022-01441) and the Swedish Strategic Research Area MERGE (Modelling the Regional and Global Earth System). Nishu Sachdeva and Johan Boman from University of Gothenburg are gratefully acknowledged for their contributions to the EDXRF analyses.

Data Availability

Measurement data from FIGAERO-I^--CIMS and EDXRF are available upon reasonable request to the corresponding authors. Data from the Sri Aurobindo Marg monitoring station is obtained from https://www.dpccairdata.com/dpccairdata/display/AallAdvanceSearchMet.php?stName=U3JpQXVy YmluZG9NYXJn. The Tropospheric Ultraviolet and Visible Radiation (TUV) Model is accessible at https://www.acom.ucar.edu/Models/TUV/Interactive_TUV. The exact sunrise and sunset time during the 2023 and 2019 campaign are retrieved from the website

https://www.timeanddate.com/sun/india/delhi.

Author Contributions

M.H., Y.C., C.W., and J.J. designed the study. E.T., J.P., C.W., R.P., and M.H. organized and performed the field observations in Delhi. R.P., H.M., G.H., and G.T. provided the measurement space, helped setting up the instruments, and facilitated the measurements. Y.C., E.T. and J.P. calibrated and quantified the data. Y.C. analyzed and visualized the data. Y.C. wrote the original draft with inputs from J.J., M.H., and C.W. All co-authors contributed to discussions and reviewing the manuscript.

Author Information

The authors declare no competing financial interests.

References

Acharja, P., Ghude, S. D., Sinha, B., Barth, M., Govardhan, G., Kulkarni, R., Sinha, V., Kumar, R., Ali, K., Gultepe, I., Petit, J.-E., and Rajeevan, M. N.: Thermodynamical framework for effective mitigation of high aerosol loading in the Indo-Gangetic Plain during winter, Scientific Reports, 13, 13667, https://doi.org/10.1038/s41598-023-40657-w, 2023.

Aggarwal, S., Bansal, P., Wang, Y., Jorga, S., Macgregor, G., Rohner, U., Bannan, T., Salter, M., Zieger, P., Mohr, C., and Lopez-Hilfiker, F.: Identifying key parameters that affect sensitivity of flow tube chemical ionization mass spectrometers, Atmospheric Measurement Techniques, 18, 4227–4247, https://doi.org/10.5194/amt-18-4227-2025, 2025.

Ahern, A. T., Goldberger, L., Jahl, L., Thornton, J., and Sullivan, R. C.: Production of N_2O_5 and $ClNO_2$ through nocturnal processing of biomass-burning aerosol, Environmental Science & Technology, 52, 550–559, https://doi.org/10.1021/acs.est.7b04386, 2018.

Ayres, B. R., Allen, H. M., Draper, D. C., Brown, S. S., Wild, R. J., Jimenez, J. L., Day, D. A., Campuzano-Jost, P., Hu, W., de Gouw, J., Koss, A., Cohen, R. C., Duffey, K. C., Romer, P., Baumann, K., Edgerton, E., Takahama, S., Thornton, J. A., Lee, B. H., Lopez-Hilfiker, F. D., Mohr, C., Wennberg, P. O., Nguyen, T. B., Teng, A., Goldstein, A. H., Olson, K., and Fry, J. L.: Organic nitrate aerosol formation via NO_3 + biogenic volatile organic compounds in the southeastern United States, Atmospheric Chemistry Physics, 15, 13377–13392, https://doi.org/10.5194/acp-15-13377-2015, 2015.

Bannan, T. J., Booth, A. M., Bacak, A., Muller, J. B. A., Leather, K. E., Le Breton, M., Jones, B., Young, D., Coe, H., Allan, J., Visser, S., Slowik, J. G., Furger, M., Prévôt, A. S. H., Lee, J., Dunmore, R. E., Hopkins, J. R., Hamilton, J. F., Lewis, A. C., Whalley, L. K., Sharp, T., Stone, D., Heard, D. E., Fleming, Z. L., Leigh, R., Shallcross, D. E., and Percival, C. J.: The first UK measurements of nitryl chloride using a chemical ionization mass spectrometer in central London in the summer of 2012, and an investigation of the role of Cl atom oxidation, Journal of Geophysical Research: Atmospheres, 120, 5638–5657, https://doi.org/10.1002/2014jd022629, 2015.

Behnke, W., George, C., Scheer, V., and Zetzsch, C.: Production and decay of $ClNO_2$ from the reaction of gaseous N_2O_5 with NaCl solution: Bulk and aerosol experiments, Journal of Geophysical Research: Atmospheres, 102, 3795–3804, https://doi.org/https://doi.org/10.1029/96JD03057, 1997.

Beig, G.: SAFAR-Delhi-2010: Development of high resolution emission inventory for National

Capital Region Delhi, Indian Institute of Tropical Meteorology (IITM), 2010.

Beig, G.: SAFAR-Delhi-2018: SAFAR-High Resolution Emission Inventory of Megacity Delhi 2018, Indian Institute of Tropical Meteorology (IITM), 2018.

Bertram, T. H., and Thornton, J. A.: Toward a general parameterization of N_2O_5 reactivity on aqueous particles: the competing effects of particle liquid water, nitrate and chloride, Atmospheric Chemistry and Physics, 9, 8351–8363, https://doi.org/10.5194/acp-9-8351-2009, 2009.

Brown, S. S., and Stutz, J.: Nighttime radical observations and chemistry, Chemical Society Reviews, 41, 6405–6447, https://doi.org/10.1039/C2CS35181A, 2012.

Bryant, D. J., Nelson, B. S., Swift, S. J., Budisulistiorini, S. H., Drysdale, W. S., Vaughan, A. R., Newland, M. J., Hopkins, J. R., Cash, J. M., Langford, B., Nemitz, E., Acton, W. J. F., Hewitt, C. N., Mandal, T., Gurjar, B. R., Shivani, Gadi, R., Lee, J. D., Rickard, A. R., and Hamilton, J. F.: Biogenic and anthropogenic sources of isoprene and monoterpenes and their secondary organic aerosol in Delhi, India, Atmospheric Chemistry and Physics, 23, 61–83, https://doi.org/10.5194/acp-23-61-2023, 2023.

Burkholder, J., Sander, S., Abbatt, J., Barker, J., Cappa, C., Crounse, J., Dibble, T., Huie, R., Kolb, C., and Kurylo, M.: Chemical kinetics and photochemical data for use in atmospheric studies, evaluation Number 19 (JPL Publication 19-5), Jet Propulsion Laboratory, Pasadena, 2020.

Chen, K., Mayorga, R., Raeofy, N., Lum, M., Woods, M., Bahreini, R., Zhang, H., and Lin, Y.-H.: Effects of nitrate radical levels and pre-existing particles on secondary brown carbon formation from nighttime oxidation of furan, ACS Earth and Space Chemistry, 6, 2709–2721, https://doi.org/10.1021/acsearthspacechem.2c00244, 2022a.

Chen, X., Xia, M., Wang, W., Yun, H., Yue, D., and Wang, T.: Fast near-surface $ClNO_2$ production and its impact on O_3 formation during a heavy pollution event in South China, Science of the Total Environment, 858, 159998, https://doi.org/10.1016/j.scitotenv.2022.159998, 2023.

Chen, X., Jiang, Y., Zong, Z., Wang, Y., Sun, W., Wang, Y., Xia, M., Guan, L., Liu, P., Zhang, C., Chen, J., Mu, Y., and Wang, T.: Atmospheric reactive halogens reshaped by the clean energy policy and agricultural activity in a rural area of the north China plain, Environmental Science & Technology, 59, 12775–12785, https://doi.org/10.1021/acs.est.4c13986, 2025a.

Chen, Y., Wang, Y., Nenes, A., Wild, O., Song, S., Hu, D., Liu, D., He, J., Hildebrandt Ruiz, L., Apte, J. S., Gunthe, S. S., and Liu, P.: Ammonium chloride associated aerosol liquid water enhances haze in Delhi, India, Environmental Science & Technology, 56, 7163–7173, https://doi.org/10.1021/acs.est.2c00650, 2022b.

Chen, Y., Xia, M., Zhang, J., Tsiligiannis, E., Wu, C., Yan, C., Cai, R., Zheng, G., Li, Y., Guo, J., An, Z., Li, Y., Zhao, X., Qu, Q., Hua, C., Wang, Z., Wang, S., Liu, Y., Cao, L., He, K., Kulmala, M., Hallquist, M., Wang, T., Worsnop, D., and Jiang, J.: Chloramine chemistry as a missing link in atmospheric chlorine cycling, Science Advances, 11, eadv4298, https://doi.org/10.1126/sciadv.adv4298, 2025b.

Dalton, E. Z., Hoffmann, E. H., Schaefer, T., Tilgner, A., Herrmann, H., and Raff, J. D.: Daytime atmospheric halogen cycling through aqueous-phase oxygen atom chemistry, Journal of the American Chemical Society, 145, 15652–15657, https://doi.org/10.1021/jacs.3c03112, 2023.

Dentener, F. J., and Crutzen, P. J.: Reaction of N_2O_5 on tropospheric aerosols: Impact on the global distributions of NO_x , O_3, and OH, Journal of Geophysical Research: Atmospheres, 98, 7149–7163,

https://doi.org/https://doi.org/10.1029/92JD02979, 1993.

Dunlea, E. J., and Ravishankara, A.: Measurement of the rate coefficient for the reaction of $O(^1D)$ with H_2O and re-evaluation of the atmospheric OH production rate, Physical Chemistry Chemical Physics, 6, 3333–3340, 2004.

Eger, P. G., Friedrich, N., Schuladen, J., Shenolikar, J., Fischer, H., Tadic, I., Harder, H., Martinez, M., Rohloff, R., Tauer, S., Drewnick, F., Fachinger, F., Brooks, J., Darbyshire, E., Sciare, J., Pikridas, M., Lelieveld, J., and Crowley, J. N.: Shipborne measurements of $ClNO_2$ in the Mediterranean Sea and around the Arabian Peninsula during summer, Atmospheric Chemistry and Physics, 19, 12121–12140, https://doi.org/10.5194/acp-19-12121-2019, 2019.

Evans, M. J., and Jacob, D. J.: Impact of new laboratory studies of N_2O_5 hydrolysis on global model budgets of tropospheric nitrogen oxides, ozone, and OH, Geophysical Research Letters, 32, L09813, https://doi.org/https://doi.org/10.1029/2005GL022469, 2005.

Fauré, N., Chen, J., Artiglia, L., Ammann, M., Bartels-Rausch, T., Kanji, Z. A., Wang, S., Pettersson, J. B. C., Thomson, E. S., Gladich, I., and Kong, X.: Formation of sodium chloride on the surface of sulfate-rich Gobi desert salt in response to water adsorption, ACS ES&T Air, 1, 1373–1382, https://doi.org/10.1021/acsestair.4c00092, 2024.

Faxon, C., Bean, J., and Ruiz, L.: Inland Concentrations of Cl_2 and $ClNO_2$ in Southeast Texas Suggest Chlorine Chemistry Significantly Contributes to Atmospheric Reactivity, Atmosphere, 6, 1487–1506, https://doi.org/10.3390/atmos6101487, 2015.

Finlayson-Pitts, B. J., Ezell, M. J., and Pitts, J. N.: Formation of chemically active chlorine compounds by reactions of atmospheric NaCl particles with gaseous N_2O_5 and $ClONO_2$, Nature, 337, 241–244, https://doi.org/10.1038/337241a0, 1989.

Gani, S., Bhandari, S., Patel, K., Seraj, S., Soni, P., Arub, Z., Habib, G., Hildebrandt Ruiz, L., and Apte, J. S.: Particle number concentrations and size distribution in a polluted megacity: the Delhi Aerosol Supersite study, Atmospheric Chemistry and Physics, 20, 8533–8549, https://doi.org/10.5194/acp-20-8533-2020, 2020.

Gunthe, S. S., Liu, P., Panda, U., Raj, S. S., Sharma, A., Darbyshire, E., Reyes-Villegas, E., Allan, J., Chen, Y., Wang, X., Song, S., Pöhlker, M. L., Shi, L., Wang, Y., Kommula, S. M., Liu, T., Ravikrishna, R., McFiggans, G., Mickley, L. J., Martin, S. T., Pöschl, U., Andreae, M. O., and Coe, H.: Enhanced aerosol particle growth sustained by high continental chlorine emission in India, Nature Geoscience, 14, 77–84, https://doi.org/10.1038/s41561-020-00677-x, 2021.

Haslett, S. L., Bell, D. M., Kumar, V., Slowik, J. G., Wang, D. S., Mishra, S., Rastogi, N., Singh, A., Ganguly, D., Thornton, J., Zheng, F., Li, Y., Nie, W., Liu, Y., Ma, W., Yan, C., Kulmala, M., Daellenbach, K. R., Hadden, D., Baltensperger, U., Prevot, A. S. H., Tripathi, S. N., and Mohr, C.: Nighttime NO emissions strongly suppress chlorine and nitrate radical formation during the winter in Delhi, Atmospheric Chemistry and Physics, 23, 9023–9036, https://doi.org/10.5194/acp-23-9023-2023, 2023.

Huang, W., Saathoff, H., Shen, X., Ramisetty, R., Leisner, T., and Mohr, C.: Chemical Characterization of Highly Functionalized Organonitrates Contributing to Night-Time Organic Aerosol Mass Loadings and Particle Growth, Environmental Science & Technology, 53, 1165–1174, https://doi.org/10.1021/acs.est.8b05826, 2019.

Huang, W., Wu, C., Gao, L., Gramlich, Y., Haslett, S. L., Thornton, J., Lopez-Hilfiker, F. D., Lee, B. H., Song, J., Saathoff, H., Shen, X., Ramisetty, R., Tripathi, S. N., Ganguly, D., Jiang, F., Vallon, M., Schobesberger, S., Yli-Juuti, T., and Mohr, C.: Variation in chemical composition and volatility of oxygenated organic aerosol in different rural, urban, and mountain environments, Atmospheric Chemistry Physics, 24, 2607–2624, https://doi.org/10.5194/acp-24-2607-2024, 2024.

Jahl, L. G., Bowers, B. B., Jahn, L. G., Thornton, J. A., and Sullivan, R. C.: Response of the reaction probability of N_2O_5 with authentic biomass-burning aerosol to high relative humidity, ACS Earth and Space Chemistry, 5, 2587–2598, https://doi.org/10.1021/acsearthspacechem.1c00227, 2021.

Jahn, L. G., McPherson, K. N., and Hildebrandt Ruiz, L.: Effects of relative humidity and photoaging on the formation, composition, and aging of ethylbenzene SOA: Insights from chamber experiments on chlorine radical-initiated oxidation of ethylbenzene, ACS Earth and Space Chemistry, 8, 675–688, https://doi.org/10.1021/acsearthspacechem.3c00279, 2024.

Jenks, O. J., DeVault, M. P., Ziola, A. C., Morris, M. A., Schueneman, M. K., Stark, H., Jimenez, J. L., Ziemann, P. J., and de Gouw, J. A.: Investigation of gas-phase products from the NO_3 radical oxidation of Δ-3-carene, ACS Earth and Space Chemistry, 7, 1097–1106, https://doi.org/10.1021/acsearthspacechem.3c00020, 2023.

Jiang, J., Carter, W. P. L., Cocker, D. R., III, and Barsanti, K. C.: Development and evaluation of a detailed mechanism for gas-phase atmospheric reactions of furans, ACS Earth and Space Chemistry, 4, 1254–1268, https://doi.org/10.1021/acsearthspacechem.0c00058, 2020.

Jimenez, J. L., Canagaratna, M. R., Donahue, N. M., Prevot, A. S. H., Zhang, Q., Kroll, J. H., DeCarlo, P. F., Allan, J. D., Coe, H., Ng, N. L., Aiken, A. C., Docherty, K. S., Ulbrich, I. M., Grieshop, A. P., Robinson, A. L., Duplissy, J., Smith, J. D., Wilson, K. R., Lanz, V. A., Hueglin, C., Sun, Y. L., Tian, J., Laaksonen, A., Raatikainen, T., Rautiainen, J., Vaattovaara, P., Ehn, M., Kulmala, M., Tomlinson, J. M., Collins, D. R., Cubison, M. J., E., Dunlea, J., Huffman, J. A., Onasch, T. B., Alfarra, M. R., Williams, P. I., Bower, K., Kondo, Y., Schneider, J., Drewnick, F., Borrmann, S., Weimer, S., Demerjian, K., Salcedo, D., Cottrell, L., Griffin, R., Takami, A., Miyoshi, T., Hatakeyama, S., Shimono, A., Sun, J. Y., Zhang, Y. M., Dzepina, K., Kimmel, J. R., Sueper, D., Jayne, J. T., Herndon, S. C., Trimborn, A. M., Williams, L. R., Wood, E. C., Middlebrook, A. M., Kolb, C. E., Baltensperger, U., and Worsnop, D. R.: Evolution of organic aerosols in the atmosphere, Science, 326, 1525–1529, https://doi.org/doi:10.1126/science.1180353, 2009.

Joo, T., Rivera-Rios, J. C., Takeuchi, M., Alvarado, M. J., and Ng, N. L.: Secondary organic aerosol formation from reaction of 3-methylfuran with nitrate radicals, ACS Earth and Space Chemistry, 3, 922–934, https://doi.org/10.1021/acsearthspacechem.9b00068, 2019.

Kashyap, P., Kumar, A., Kumar, R. P., and Kumar, K.: Biogenic and anthropogenic isoprene emissions in the subtropical urban atmosphere of Delhi, Atmospheric Pollution Research, 10, 1691–1698, https://doi.org/https://doi.org/10.1016/j.apr.2019.07.004, 2019.

Kenagy, H. S., Heald, C. L., Tahsini, N., Goss, M. B., and Kroll, J. H.: Can we achieve atmospheric chemical environments in the laboratory? An integrated model-measurement approach to chamber SOA studies, Science Advances, 10, eado1482, https://doi.org/10.1126/sciadv.ado1482, 2024.

Kercher, J. P., Riedel, T. P., and Thornton, J. A.: Chlorine activation by N_2O_5: Simultaneous, in situ detection of $ClNO_2$ and N_2O_5 by chemical ionization mass spectrometry, Atmospheric

Measurement Techniques, 2, 193–204, https://doi.org/10.5194/amt-2-193-2009, 2009.

Kumar, V., Giannoukos, S., Haslett, S. L., Tong, Y., Singh, A., Bertrand, A., Lee, C. P., Wang, D. S., Bhattu, D., Stefenelli, G., Dave, J. S., Puthussery, J. V., Qi, L., Vats, P., Rai, P., Casotto, R., Satish, R., Mishra, S., Pospisilova, V., Mohr, C., Bell, D. M., Ganguly, D., Verma, V., Rastogi, N., Baltensperger, U., Tripathi, S. N., Prévôt, A. S. H., and Slowik, J. G.: Highly time-resolved chemical speciation and source apportionment of organic aerosol components in Delhi, India, using extractive electrospray ionization mass spectrometry, Atmospheric Chemistry and Physics, 22, 7739–7761, https://doi.org/10.5194/acp-22-7739-2022, 2022.

Le Breton, M., Hallquist, Å. M., Pathak, R. K., Simpson, D., Wang, Y., Johansson, J., Zheng, J., Yang, Y., Shang, D., Wang, H., Liu, Q., Chan, C., Wang, T., Bannan, T. J., Priestley, M., Percival, C. J., Shallcross, D. E., Lu, K., Guo, S., Hu, M., and Hallquist, M.: Chlorine oxidation of VOCs at a semi-rural site in Beijing: Significant chlorine liberation from $ClNO_2$ and subsequent gas- and particle-phase Cl–VOC production, Atmospheric Chemistry and Physics, 18, 13013–13030, https://doi.org/10.5194/acp-18-13013-2018, 2018a.

Le Breton, M., Wang, Y., Hallquist, Å. M., Pathak, R. K., Zheng, J., Yang, Y., Shang, D., Glasius, M., Bannan, T. J., Liu, Q., Chan, C. K., Percival, C. J., Zhu, W., Lou, S., Topping, D., Wang, Y., Yu, J., Lu, K., Guo, S., Hu, M., and Hallquist, M.: Online gas- and particle-phase measurements of organosulfates, organosulfonates and nitrooxy organosulfates in Beijing utilizing a FIGAERO ToF-CIMS, Atmospheric Chemistry and Physics, 18, 10355–10371, https://doi.org/10.5194/acp-18-10355-2018, 2018b.

Li, M., Xia, M., Lin, C., Jiang, Y., Sun, W., Wang, Y., Zhang, Y., He, M., and Wang, T.: Mechanistic insights into chloroacetic acid production from atmospheric multiphase volatile organic compound-chlorine chemistry, Atmospheric Chemistry and Physics, 25, 3753–3764, https://doi.org/10.5194/acp-25-3753-2025, 2025.

Lim, Y. B., and Ziemann, P. J.: Chemistry of secondary organic aerosol formation from OH radical-initiated reactions of linear, branched, and cyclic alkanes in the presence of NO_x, Aerosol Science and Technology, 43, 604–619, https://doi.org/10.1080/02786820902802567, 2009.

Liu, X., Qu, H., Huey, L. G., Wang, Y., Sjostedt, S., Zeng, L., Lu, K., Wu, Y., Hu, M., Shao, M., Zhu, T., and Zhang, Y.: High levels of daytime molecular chlorine and nitryl chloride at a rural site on the North China Plain, Environmental Science & Technology, 51, 9588–9595, https://doi.org/10.1021/acs.est.7b03039, 2017.

Ljungström, E., and Hallquist, M.: Nitrate radical formation rates in scandinavia, Atmospheric Environment, 30, 2925–2932, https://doi.org/https://doi.org/10.1016/1352-2310(96)00006-4, 1996.

Lopez-Hilfiker, F. D., Mohr, C., Ehn, M., Rubach, F., Kleist, E., Wildt, J., Mentel, T. F., Lutz, A., Hallquist, M., Worsnop, D., and Thornton, J. A.: A novel method for online analysis of gas and particle composition: description and evaluation of a Filter Inlet for Gases and AEROsols (FIGAERO), Atmospheric Measurement Techniques, 7, 983–1001, https://doi.org/10.5194/amt-7-983-2014, 2014.

Ma, W., Chen, X., Xia, M., Liu, Y., Wang, Y., Zhang, Y., Zheng, F., Zhan, J., Hua, C., Wang, Z., Wang, W., Fu, P., Kulmala, M., and Liu, Y.: Reactive chlorine species advancing the atmospheric oxidation capacities of inland urban environments, Environmental Science & Technology, 57, 14638–14647, https://doi.org/10.1021/acs.est.3c05169, 2023.

Margerum, D. W., Schurter, L. M., Hobson, J., and Moore, E. E.: Water chlorination chemistry: Nonmetal redox kinetics of chloramine and nitrite ion, Environmental Science & Technology, 28, 331–337, 1994.

McNamara, S. M., AR, W. R., Wang, S., Thanekar, S., Boone, E. J., Kolesar, K. R., Peterson, P. K., Simpson, W. R., Fuentes, J. D., Shepson, P. B., and Pratt, K. A.: Springtime nitrogen oxide-influenced chlorine chemistry in the coastal Arctic, Environmental Science & Technology, 53, 8057–8067, https://doi.org/10.1021/acs.est.9b01797, 2019.

McNamara, S. M., Kolesar, K. R., Wang, S., Kirpes, R. M., May, N. W., Gunsch, M. J., Cook, R. D., Fuentes, J. D., Hornbrook, R. S., Apel, E. C., China, S., Laskin, A., and Pratt, K. A.: Observation of road salt aerosol driving inland wintertime atmospheric chlorine chemistry, ACS Central Science, 6, 684–694, https://doi.org/10.1021/acscentsci.9b00994, 2020.

Meidan, D., Brown, S. S., Sinha, V., and Rudich, Y.: Nocturnal atmospheric oxidative processes in the Indo-Gangetic plain and their variation during the COVID-19 lockdowns, Geophysical Research Letters, 49, e2021GL097472, https://doi.org/10.1029/2021GL097472, 2022.

Mielke, L. H., Stutz, J., Tsai, C., Hurlock, S. C., Roberts, J. M., Veres, P. R., Froyd, K. D., Hayes, P. L., Cubison, M. J., Jimenez, J. L., Washenfelder, R. A., Young, C. J., Gilman, J. B., Gouw, J. A., Flynn, J. H., Grossberg, N., Lefer, B. L., Liu, J., Weber, R. J., and Osthoff, H. D.: Heterogeneous formation of nitryl chloride and its role as a nocturnal NO_x reservoir species during CalNex-LA 2010, Journal of Geophysical Research: Atmospheres, 118, 10638–10652, https://doi.org/10.1002/jgrd.50783, 2013.

Mishra, S., Sinha, V., Hakkim, H., Awasthi, A., Ghude, S. D., Soni, V. K., Nigam, N., Sinha, B., and Rajeevan, M. N.: Reactive chlorine-, sulfur-, and nitrogen-containing volatile organic compounds impact atmospheric chemistry in the megacity of Delhi during both clean and extremely polluted seasons, Atmospheric Chemistry and Physics, 24, 13129–13150, https://doi.org/10.5194/acp-24-13129-2024, 2024.

Nelson, B. S., Stewart, G. J., Drysdale, W. S., Newland, M. J., Vaughan, A. R., Dunmore, R. E., Edwards, P. M., Lewis, A. C., Hamilton, J. F., Acton, W. J., Hewitt, C. N., Crilley, L. R., Alam, M. S., Şahin, Ü. A., Beddows, D. C. S., Bloss, W. J., Slater, E., Whalley, L. K., Heard, D. E., Cash, J. M., Langford, B., Nemitz, E., Sommariva, R., Cox, S., Shivani, Gadi, R., Gurjar, B. R., Hopkins, J. R., Rickard, A. R., and Lee, J. D.: In situ ozone production is highly sensitive to volatile organic compounds in Delhi, India, Atmospheric Chemistry and Physics, 21, 13609–13630, https://doi.org/10.5194/acp-21-13609-2021, 2021.

Noxon, J. F., Norton, R. B., and Marovich, E.: NO_3 in the troposphere, Geophysical Research Letters, 7, 125–128, https://doi.org/https://doi.org/10.1029/GL007i002p00125, 1980.

Ogrizek, M., Kroflič, A., and Šala, M.: Critical review on the development of analytical techniques for the elemental analysis of airborne particulate matter, Trends in Environmental Analytical Chemistry, 33, e00155, https://doi.org/https://doi.org/10.1016/j.teac.2022.e00155, 2022.

Osthoff, H. D., Roberts, J. M., Ravishankara, A. R., Williams, E. J., Lerner, B. M., Sommariva, R., Bates, T. S., Coffman, D., Quinn, P. K., Dibb, J. E., Stark, H., Burkholder, J. B., Talukdar, R. K., Meagher, J., Fehsenfeld, F. C., and Brown, S. S.: High levels of nitryl chloride in the polluted subtropical marine boundary layer, Nature Geoscience, 1, 324–328, https://doi.org/10.1038/ngeo177,

2008.

Patel, A., Reddy, M. C., Zhang, B., Swain, B., Pandithurai, G., Andreae, M. O., Martin, S. T., Liu, P., and Gunthe, S. S.: Linking anthropogenic chlorine emissions to regional air quality in India, npj Clean Air, 2, 23, https://doi.org/10.1038/s44407-026-00066-5, 2026.

Peng, X., Wang, W., Xia, M., Chen, H., Ravishankara, A. R., Li, Q., Saiz-Lopez, A., Liu, P., Zhang, F., Zhang, C., Xue, L., Wang, X., George, C., Wang, J., Mu, Y., Chen, J., and Wang, T.: An unexpected large continental source of reactive bromine and chlorine with significant impact on wintertime air quality, National Science Review 8, nwaa304, https://doi.org/10.1093/nsr/nwaa304, 2021.

Phillips, G. J., Tang, M. J., Thieser, J., Brickwedde, B., Schuster, G., Bohn, B., Lelieveld, J., and Crowley, J. N.: Significant concentrations of nitryl chloride observed in rural continental Europe associated with the influence of sea salt chloride and anthropogenic emissions, Geophysical Research Letters, 39, L10811, https://doi.org/10.1029/2012gl051912, 2012.

Priestley, M., le Breton, M., Bannan, T. J., Worrall, S. D., Bacak, A., Smedley, A. R. D., Reyes-Villegas, E., Mehra, A., Allan, J., Webb, A. R., Shallcross, D. E., Coe, H., and Percival, C. J.: Observations of organic and inorganic chlorinated compounds and their contribution to chlorine radical concentrations in an urban environment in northern Europe during the wintertime, Atmospheric Chemistry and Physics, 18, 13481–13493, https://doi.org/10.5194/acp-18-13481-2018, 2018.

Raff, J. D., Njegic, B., Chang, W. L., Gordon, M. S., Dabdub, D., Gerber, R. B., and Finlayson-Pitts, B. J.: Chlorine activation indoors and outdoors via surface-mediated reactions of nitrogen oxides with hydrogen chloride, Proceedings of the National Academy of Sciences, 106, 13647–13654, https://doi.org/doi:10.1073/pnas.0904195106, 2009.

Rai, P., Furger, M., El Haddad, I., Kumar, V., Wang, L., Singh, A., Dixit, K., Bhattu, D., Petit, J.-E., Ganguly, D., Rastogi, N., Baltensperger, U., Tripathi, S. N., Slowik, J. G., and Prévôt, A. S. H.: Real-time measurement and source apportionment of elements in Delhi's atmosphere, Science of the Total Environment, 742, 140332, https://doi.org/https://doi.org/10.1016/j.scitotenv.2020.140332, 2020.

Riedel, T. P., Bertram, T. H., Crisp, T. A., Williams, E. J., Lerner, B. M., Vlasenko, A., Li, S. M., Gilman, J., de Gouw, J., Bon, D. M., Wagner, N. L., Brown, S. S., and Thornton, J. A.: Nitryl chloride and molecular chlorine in the coastal marine boundary layer, Environmental Science & Technology, 46, 10463–10470, https://doi.org/10.1021/es204632r, 2012.

Sahu, S. K., Mangaraj, P., and Beig, G.: Decadal growth in emission load of major air pollutants in Delhi, Earth System Science Data, 15, 3183–3202, https://doi.org/10.5194/essd-15-3183-2023, 2023.

Simpson, W. R., Brown, S. S., Saiz-Lopez, A., Thornton, J. A., and Glasow, R.: Tropospheric halogen chemistry: Sources, cycling, and impacts, Chemical Reviews, 115, 4035–4062, https://doi.org/10.1021/cr5006638, 2015.

Soni, M., Sander, R., Sahu, L. K., Taraborrelli, D., Liu, P., Patel, A., Girach, I. A., Pozzer, A., Gunthe, S. S., and Ojha, N.: Comprehensive multiphase chlorine chemistry in the box model CAABA/MECCA: Implications for atmospheric oxidative capacity, Atmospheric Chemistry and Physics, 23, 15165–15180, https://doi.org/10.5194/acp-23-15165-2023, 2023.

Tham, Y. J., Wang, Z., Li, Q., Yun, H., Wang, W., Wang, X., Xue, L., Lu, K., Ma, N., Bohn, B., Li, X., Kecorius, S., Größ, J., Shao, M., Wiedensohler, A., Zhang, Y., and Wang, T.: Significant

concentrations of nitryl chloride sustained in the morning: Investigations of the causes and impacts on ozone production in a polluted region of northern China, Atmospheric Chemistry and Physics, 16, 14959–14977, https://doi.org/10.5194/acp-16-14959-2016, 2016.

Tham, Y. J., Wang, Z., Li, Q., Wang, W., Wang, X., Lu, K., Ma, N., Yan, C., Kecorius, S., Wiedensohler, A., Zhang, Y., and Wang, T.: Heterogeneous N_2O_5 uptake coefficient and production yield of $ClNO_2$ in polluted northern China: Roles of aerosol water content and chemical composition, Atmospheric Chemistry and Physics, 18, 13155–13171, https://doi.org/10.5194/acp-18-13155-2018, 2018.

Thornton, J. A., Braban, C. F., and Abbatt, J. P. D.: N_2O_5 hydrolysis on sub-micron organic aerosols: the effect of relative humidity, particle phase, and particle size, Physical Chemistry Chemical Physics, 5, 4593–4603, https://doi.org/10.1039/B307498F, 2003.

Thornton, J. A., and Abbatt, J. P. D.: N_2O_5 reaction on submicron sea salt aerosol: Kinetics, products, and the effect of surface active organics, The Journal of Physical Chemistry A, 109, 10004–10012, https://doi.org/10.1021/jp054183t, 2005.

Thornton, J. A., Kercher, J. P., Riedel, T. P., Wagner, N. L., Cozic, J., Holloway, J. S., Dube, W. P., Wolfe, G. M., Quinn, P. K., Middlebrook, A. M., Alexander, B., and Brown, S. S.: A large atomic chlorine source inferred from mid-continental reactive nitrogen chemistry, Nature, 464, 271–274, https://doi.org/10.1038/nature08905, 2010.

Trebs, I., Bohn, B., Ammann, C., Rummel, U., Blumthaler, M., Königstedt, R., Meixner, F. X., Fan, S., and Andreae, M. O.: Relationship between the NO_2 photolysis frequency and the solar global irradiance, Atmospheric Measurement Techniques, 2, 725–739, https://doi.org/10.5194/amt-2-725-2009, 2009.

Unga, F., Calzolai, G., Chiari, M., Cuccia, E., Colombi, C., Franciosa, M., Dinoi, A., Merico, E., Pennetta, A., Gómez-Sánchez, N., Mapelli, C., Pareti, S., Perrino, C., Yubero, E., and Contini, D.: Determination of aerosol composition by ED-XRF on Teflon and quartz substrates: potentialities and limits, Aerosol Research, 3, 405–415, https://doi.org/10.5194/ar-3-405-2025, 2025.

Wang, C., Liggio, J., Wentzell, J. J. B., Jorga, S., Folkerson, A., and Abbatt, J. P. D.: Chloramines as an important photochemical source of chlorine atoms in the urban atmosphere, Proceedings of the National Academy of Sciences of the United States of America, 120, e2220889120, https://doi.org/doi:10.1073/pnas.2220889120, 2023a.

Wang, D. S., and Hildebrandt Ruiz, L.: Chlorine-initiated oxidation of n-alkanes under high-NO_x conditions: Insights into secondary organic aerosol composition and volatility using a FIGAERO-CIMS, Atmospheric Chemistry and Physics, 18, 15535–15553, https://doi.org/10.5194/acp-18-15535-2018, 2018.

Wang, D. S., Masoud, C. G., Modi, M., and Hildebrandt Ruiz, L.: Isoprene-chlorine oxidation in the presence of NO_x and implications for urban atmospheric chemistry, Environmental Science & Technology, 56, 9251–9264, https://doi.org/10.1021/acs.est.1c07048, 2022.

Wang, H., Lu, K., Chen, X., Zhu, Q., Chen, Q., Guo, S., Jiang, M., Li, X., Shang, D., Tan, Z., Wu, Y., Wu, Z., Zou, Q., Zheng, Y., Zeng, L., Zhu, T., Hu, M., and Zhang, Y.: High N_2O_5 concentrations observed in urban Beijing: Implications of a large nitrate formation pathway, Environmental Science & Technology Letters, 4, 416–420, https://doi.org/10.1021/acs.estlett.7b00341, 2017.

Wang, H., Wang, H., Lu, X., Lu, K., Zhang, L., Tham, Y. J., Shi, Z., Aikin, K., Fan, S., Brown, S. S., and Zhang, Y.: Increased night-time oxidation over China despite widespread decrease across the globe, Nature Geoscience, 16, 217–223, https://doi.org/10.1038/s41561-022-01122-x, 2023b.

Wang, J., Wang, H., Tham, Y. J., Ming, L., Zheng, Z., Fang, G., Sun, C., Ling, Z., Zhao, J., and Fan, S.: Measurement report: Atmospheric nitrate radical chemistry in the South China Sea influenced by the urban outflow of the Pearl River Delta, Atmospheric Chemistry and Physics, 24, 977–992, https://doi.org/10.5194/acp-24-977-2024, 2024.

Wang, L., Slowik, J. G., Tripathi, N., Bhattu, D., Rai, P., Kumar, V., Vats, P., Satish, R., Baltensperger, U., Ganguly, D., Rastogi, N., Sahu, L. K., Tripathi, S. N., and Prévôt, A. S. H.: Source characterization of volatile organic compounds measured by proton-transfer-reaction time-of-flight mass spectrometers in Delhi, India, Atmospheric Chemistry and Physics, 20, 9753–9770, https://doi.org/10.5194/acp-20-9753-2020, 2020.

Wang, T., Brown, S. S., Dubé, W. P., Tham, Y. J., Zha, Q., Xue, L., Poon, S., Wang, Z., Blake, D. R., Tsui, W., and Parrish, D. D.: Observations of nitryl chloride and modeling its source and effect on ozone in the planetary boundary layer of southern China, Journal of Geophysical Research: Atmospheres, 121, 2457–2475, https://doi.org/10.1002/2015jd024566, 2016.

Wang, X., Jacob, D. J., Eastham, S. D., Sulprizio, M. P., Zhu, L., Chen, Q., Alexander, B., Sherwen, T., Evans, M. J., Lee, B. H., Haskins, J. D., Lopez-Hilfiker, F. D., Thornton, J. A., Huey, G. L., and Liao, H.: The role of chlorine in global tropospheric chemistry, Atmospheric Chemistry and Physics, 19, 3981–4003, https://doi.org/10.5194/acp-19-3981-2019, 2019.

Wängberg, I., Etzkorn, T., Barnes, I., Platt, U., and Becker, K. H.: Absolute determination of the temperature behavior of the $NO_2 + NO_3 + (M) \leftrightarrow N_2O_5 + (M)$ equilibrium, The Journal of Physical Chemistry A, 101, 9694–9698, https://doi.org/10.1021/jp972203o, 1997.

Xia, M., Peng, X., Wang, W., Yu, C., Sun, P., Li, Y., Liu, Y., Xu, Z., Wang, Z., Xu, Z., Nie, W., Ding, A., and Wang, T.: Significant production of $ClNO_2$ and possible source of Cl_2 from N_2O_5 uptake at a suburban site in eastern China, Atmospheric Chemistry and Physics, 20, 6147–6158, https://doi.org/10.5194/acp-20-6147-2020, 2020.

Xia, M., Peng, X., Wang, W., Yu, C., Wang, Z., Tham, Y. J., Chen, J., Chen, H., Mu, Y., Zhang, C., Liu, P., Xue, L., Wang, X., Gao, J., Li, H., and Wang, T.: Winter $ClNO_2$ formation in the region of fresh anthropogenic emissions: seasonal variability and insights into daytime peaks in northern China, Atmospheric Chemistry and Physics, 21, 15985–16000, https://doi.org/10.5194/acp-21-15985-2021, 2021.

Xia, M., Jiang, Y., Dai, J., Liu, Y., Yan, C., Kulmala, M., and Wang, T.: Chlorine activation in marine air: Insights from chemical budgets of molecular chlorine and hypochlorous acid, Journal of Geophysical Research: Atmospheres, 130, e2024JD042568, https://doi.org/https://doi.org/10.1029/2024JD042568, 2025.

Xu, T., Takeuchi, M., Rivera-Rios, J. C., and Ng, N. L.: Multigeneration Chemistry in Secondary Organic Aerosol Formation from Nitrate Radical Oxidation of Isoprene, ACS Earth and Space Chemistry, 9, 411–423, https://doi.org/10.1021/acsearthspacechem.4c00417, 2025.

Yan, C., Tham, Y. J., Nie, W., Xia, M., Wang, H., Guo, Y., Ma, W., Zhan, J., Hua, C., Li, Y., Deng, C., Li, Y., Zheng, F., Chen, X., Li, Q., Zhang, G., Mahajan, A. S., Cuevas, C. A., Huang, D. D., Wang,

Z., Sun, Y., Saiz-Lopez, A., Bianchi, F., Kerminen, V.-M., Worsnop, D. R., Donahue, N. M., Jiang, J., Liu, Y., Ding, A., and Kulmala, M.: Increasing contribution of nighttime nitrogen chemistry to wintertime haze formation in Beijing observed during COVID-19 lockdowns, Nature Geoscience, https://doi.org/10.1038/s41561-023-01285-1, 2023.

Yan, Y., Wang, S., Zhu, J., Guo, Y., Tang, G., Liu, B., An, X., Wang, Y., and Zhou, B.: Vertically increased NO_3 radical in the nocturnal boundary layer, Science of the Total Environment, 763, 142969, https://doi.org/https://doi.org/10.1016/j.scitotenv.2020.142969, 2021.

Yang, X., Wang, Q., Ma, N., Hu, W., Gao, Y., Huang, Z., Zheng, J., Yuan, B., Yang, N., Tao, J., Hong, J., Cheng, Y., and Su, H.: The impact of chlorine chemistry combined with heterogeneous N_2O_5 reactions on air quality in China, Atmospheric Chemistry and Physics, 22, 3743–3762, https://doi.org/10.5194/acp-22-3743-2022, 2022.

Ye, C., Yuan, B., Lin, Y., Wang, Z., Hu, W., Li, T., Chen, W., Wu, C., Wang, C., Huang, S., Qi, J., Wang, B., Wang, C., Song, W., Wang, X., Zheng, E., Krechmer, J. E., Ye, P., Zhang, Z., Wang, X., Worsnop, D. R., and Shao, M.: Chemical characterization of oxygenated organic compounds in the gas phase and particle phase using iodide CIMS with FIGAERO in urban air, Atmospheric Chemistry and Physics, 21, 8455–8478, https://doi.org/10.5194/acp-21-8455-2021, 2021.

Zhang, T., Zuo, P., Chen, Y., Liu, T., Zeng, L., Lin, W., and Ye, C.: Measurement report: Variations and environmental impacts of atmospheric N_2O_5 concentrations in urban Beijing during the 2022 Winter Olympics, Atmospheric Chemistry and Physics, 25, 16331–16346, https://doi.org/10.5194/acp-25-16331-2025, 2025.

Zhou, W., Zhao, J., Ouyang, B., Mehra, A., Xu, W., Wang, Y., Bannan, T. J., Worrall, S. D., Priestley, M., Bacak, A., Chen, Q., Xie, C., Wang, Q., Wang, J., Du, W., Zhang, Y., Ge, X., Ye, P., Lee, J. D., Fu, P., Wang, Z., Worsnop, D., Jones, R., Percival, C. J., Coe, H., and Sun, Y.: Production of N_2O_5 and $ClNO_2$ in summer in urban Beijing, China, Atmospheric Chemistry and Physics, 18, 11581–11597, https://doi.org/10.5194/acp-18-11581-2018, 2018.

Supporting Information of

Enhanced nocturnal N_2O_5-$ClNO_2$ chemistry in Delhi under reduced NO conditions

Yijing Chen[1,2], Cheng Wu[2]*, Epameinondas Tsiligiannis[2], Ravi Kant Pathak[2,3], Jan B. C. Pettersson[2], Harsh Raj Mishra[2,3]†, Gazala Habib[4], Geetam Tiwari[5], Kebin He[1], Jingkun Jiang[1]*, Mattias Hallquist[2]*

Affiliations:

[1]State Key Laboratory of Regional Environment and Sustainability, School of Environment, Tsinghua University, Beijing, 100084, China.

[2]Department of Chemistry and Molecular Biology, University of Gothenburg, Gothenburg, 40530, Sweden.

[3]Indo-Gangetic Plains Centre for Air Research and Education (IGP-CARE), Hamirpur, Uttar Pradesh, 210301, India.

[4]Transportation Research and Injury Prevention Centre, Indian Institute of Technology Delhi, New Delhi, 110016, India.

[5]Department of Civil Engineering, Indian Institute of Technology Delhi, New Delhi, 110016, India.

†Present address: School of Earth and Atmospheric Sciences, Queensland University of Technology, Queensland, 4001, Brisbane, Australia.

***Correspondence to:** Mattias Hallquist (hallq@chem.gu.se), Jingkun Jiang (jiangjk@tsinghua.edu.cn) and Cheng Wu (cheng.wu@gu.se).

This PDF file includes:

Text S1 to S2
Figures S1 to S20
Table S1 to S4

Text. S1 Details of field measurements in Delhi

1.1 FIGAERO-I^--CIMS configurations

The reagent ions (I^- and $I \cdot H_2O^-$) were produced by passing ~2 lpm ultrahigh purity (UHP) N_2 via a CH_3I permeation tube and through a Po-210 ion source, where it interacted with the sampled air or thermally desorbed molecules from $PM_{2.5}$ in the ion-molecular reactor (IMR). A constant 10 sccm of H_2O-saturated UHP was added directly into the IMR to reduce the sensitivity variability with ambient RH. The IMR pressure was maintained at 200-250 mbar during gas sampling and 120-140 mbar during $PM_{2.5}$ desorption. The relatively lower pressure during the $PM_{2.5}$ measurement was likely caused by the resistance and associated pressure drop across the filters. Considering the differences in IMR pressures, we conducted sensitivity calibrations for the gas- and particle-phase measurements separately under conditions similar to the field observations in Delhi. The average mass resolution was ~3500 at m/z 127.

For gas-phase measurements, ambient air was drawn at 3 lpm through a 4-m-long PFA tube (inner diameter, 5 mm, residence time 1.6 s) with 2 lpm pumped away. An impactor with a cut-off of $PM_{2.5}$ was placed at the gas inlet to reduce large particles deposited in the sampling system. The bypass flow was utilized to ensure a short residence time (~1.6 s) while maintaining a laminar flow (Reynolds number = 840 <2300) within the tubing, thereby suppressing both wall loss and gas-particle reactions within the inlet. The remaining 1 lpm was diluted with 1 lpm UHP N_2 before entering the IMR to avoid reagent ion titration by high levels of pollutants (e.g., HNO_3) in the ambient air.

For background measurements, the inlet was flushed with ~2 lpm UHP N_2 during the first and last two minutes of each 20-min gas-phase measurement to obtain background signals, while ambient sampling was performed during the remaining period. Continuous and automated background measurements were achieved with this flow rate configuration. The signals from the second zeroing period were used as the background, since those from the first zeroing period may have been influenced by carryover desorption signals (especially for sticky compounds) from the preceding particle-phase measurement (Fig. S5). The background-subtracted and dilution ratio (a factor of 2) corrected ion signals were subsequently averaged to 1-hour intervals.

For $PM_{2.5}$ measurements, ambient air was drawn at 3 lpm through a 4-m-long copper tube (inner diameter, 5 mm) fitted with a $PM_{2.5}$ cyclone during the gas-sampling period, with 2 lpm discarded and 1 lpm collected on a Teflon filter for 20 min. The filter was then moved to the desorption position, where it was thermally desorbed and carried into the IMR under a 2 lpm flow of UHP N_2. The N_2 flow was gradually ramped from

room temperature to 200 ℃ in 20 min, soaked at 200 ℃ for 20 min, and finally cooled back to room temperature in 10 min. The particle phase signal was integrated over the temperature ramping and soaking period during filter desorption. The baseline was determined from linear fitting of the signal between the onset of heating and the end of soaking and was integrated and subtracted from the integrated desorption signals.

1.2. Sensitivity calibrations of N_2O_5, $ClNO_2$ and related species

N_2O_5 and $ClNO_2$. N_2O_5 was prepared by mixing O_3 with excessive NO_2 to promote the conversion of NO_3 to N_2O_5. The generated N_2O_5 concentrations were determined by the change in O_3 following the addition of NO_2, and different N_2O_5 levels were achieved via varying O_3 concentration (Bertram et al., 2009). The produced N_2O_5 was further diluted with humidified zero air to approximate Delhi RH conditions before entering the CIMS. $ClNO_2$ was produced by passing a known amount of N_2O_5 through a wetted NaCl-slurry placed in a Teflon tube, assuming a unit conversion from N_2O_5 to $ClNO_2$ (Finlayson-Pitts, 2003). All the tubing is covered by aluminum foil to avoid NO_3 photolysis and were flushed with dry zero air overnight before calibration to minimize potential N_2O_5 hydrolysis on the tubing surfaces. The calibration curve for N_2O_5 and $ClNO_2$ are shown in Fig. S19a-b**.** No water-dependent sensitivity correction was applied for N_2O_5 and $ClNO_2$, as no significant sensitivity variation was observed in the range of $H_2O{\cdot}I^-/I^-$ ratios during the field measurements in Delhi (Fig. S19c-d**)**.

HCl and chloroacetic acid. A certified 10 ppm HCl gas cylinder (Linde Specialgas) was used as the standard source, which was diluted with zero air to different mixing ratios before introducing to the CIMS (Fig. S19e). We observed a significant decrease of the HCl sensitivity at high $H_2O{\cdot}I^-/I^-$ ratios (Fig. S19f), likely due to the competing effects of H_2O for clustering with iodide anion and that the reaction of HCl with $H_2O{\cdot}I^-$ is thermodynamically less favorable compared to reacting with iodide anion. The slight increase in HCl sensitivity with increasing $H_2O{\cdot}I^-/I^-$ ratio at low RH levels may be related to the stabilization of $HCl{\cdot}I^-$ clusters by water vapors. Similar patterns have been reported for other acids in a previous study (Lee et al., 2014). Gaseous chloroacetic acid was generated by placing solid chloroacetic acid in a glass vial submerged in a 30 °C water bath. The emission rate, determined by gravimetric weight loss analysis, was 177.3 ± 0.8 ng/min. No significant H_2O dependence of chloroacetic acid sensitivity was observed. It is noted that HCl was calibrated in the concentration range about 2~3 orders of magnitude higher than the ambient level. Nevertheless, given the strong linearity of the multipoint calibration at high HCl concentrations, and the verified linear response of the CIMS at lower concentrations for N_2O_5 and $ClNO_2$, we assume that the calibrated HCl sensitivity is applicable to ambient measurements.

Levoglucosan. A certain amount (10~90 ng) of levoglucosan dissolved in acetone solutions was deposited on the filter of the CIMS, and then the droplet underwent the same thermal desorption cycle as in the field measurements. The sensitivity for levoglucosan was derived as the integrated background-subtracted signals divided by the deposited mass.

1.3. R.K. Puram station data quality control

Hourly pollutant measurements from the R.K. Puram station were obtained to examine the long-term pollutant trends in Delhi. We applied rigorous data quality controls following recent studies (Vohra et al., 2025;Xie et al., 2024) with a few modifications, including (1) Remove duplicates: In sequences of five or more consecutive identical hourly values, only the first value out of the sequence is retained, (2) Remove outliers: For a 24-h running window, flag any observation as an outlier if its absolute difference from the median exceeds three times the Median Absolute Deviation (MAD, median distance between each observation and the median of all observations), (3) Remove constant data: In a 24-h running window, remove constant data values with coefficient of variation (ratio of standard deviation to the mean) less than 5%, (4) Validation of NO, NO_2 measurements by comparing with the measured NO_x: consider NO and NO_2 are reported correctly in units of μg/m^3 and assess if NO_x calculated from these is within 2% of reported NO_x + 2.5 ppb. If not, the measured NO, NO_2, and NO_x data were omitted.

Text. S2 Estimation of the N_2O_5 uptake coefficient

2.1 Inapplicability of the steady-state method

The steady-state approximation of the NO_2-NO_3-N_2O_5 system is a widely applied method (Brown et al., 2003) for estimating the values for the NO_3 and N_2O_5 sinks (thereby $\gamma_{N_2O_5}$) in various atmospheric environments (Brown et al., 2006;Wang et al., 2017b;Wang et al., 2017a). This method assumes that production rate of NO_3 and N_2O_5 equals the sum of the loss rates during a certain period of the night (Eq. S1), and therefore k_{NO_3} and $k_{N_2O_5}$ can be determined as the slope and intercept, respectively, of the linear fitting between ${\tau_{N_2O_5}}^{-1}$ and $\frac{1}{K_{eq}[NO_2]}$ (Eq. S2). However, we found no siginificant positive or even negative correlation between ${\tau_{N_2O_5}}^{-1}$ and $\frac{1}{K_{eq}[NO_2]}$ during the nighttime throughout the campaign (an example is shown in Fig. S20). This is likely attributed to the intense and variable NO_x emissions in Delhi (avg. nighttime hourly NO_x mixing ratios of 92 ± 60 ppb) which preclude the system from approaching steady-state on the time-scale of a night. As is in shown in Fig. 2a of the main text, N_2O_5 presented a strong negative dependence on NO. The high

concentrations and large flucuations of NO dominated the variation of N_2O_5, thereby decoupling the lifetime of N_2O_5 from $\frac{1}{K_{eq}[NO_2]}$.

$$k_{NO_2+O_3}[NO_2][O_3] = k_{NO_3}[NO_3] + k_{N_2O_5}[N_2O_5] \ (Eq.\ S1)$$

Substitute $[NO_3] = \frac{[N_2O_5]}{K_{eq}[NO_2]}$ to $Eq.\ S1$, we get

$$\tau_{N_2O_5}{}^{-1} = \frac{k_{NO_2+O_3}[NO_2][O_3]}{[N_2O_5]} = \frac{k_{NO_3}}{K_{eq}[NO_2]} + k_{N_2O_5} \ (Eq.\ S2)$$

Where k_{NO_3} and $k_{N_2O_5}$ are the pseudo-first-order loss rate constants of NO_3 and N_2O_5, respectively, K_{eq} is the equilibrium constant of the NO_2-NO_3-N_2O_5 system, where $K_{eq} = 5.5 \times 10^{-2} \times \exp(10724/T)$, $k_{N_2O_5} = \frac{\bar{c}\gamma}{4} S_a$, $\tau_{N_2O_5}{}^{-1}$ is the inverse of the N_2O_5 steady-state lifetime.

2.2 Validation of the RH parameterization method

$ClNO_2$ yield indicates the branching ratio of $H_2ONO_2^+$ reacting with H_2O (R4) and chloride (R5), which is theoretically determined by the respective reaction rates shown in Eq. S3 (Bertram and Thornton, 2009).

$$f_{ClNO_2} = \frac{k_{R5}[H_2ONO_2^+][Cl^-]}{k_{R5}[H_2ONO_2^+][Cl^-] + k_{R4}[H_2ONO_2^+][H_2O]} = \frac{1}{1 + \frac{k_{R4}}{k_{R5}}\frac{[H_2O]}{[Cl^-]}} \ (Eq.\ S3)$$

Where $[H_2O]$ and $[Cl^-]$ are molar concentrations in the aqueous phase of particles derived from thermodynamic models, k_{R5} and k_{R4} are reaction rate coefficients of Reaction R5 and R4. The experimentally determined value for k_{R5}/k_{R4} is 483±175 from the work of Bertram and Thornton (Bertram and Thornton, 2009) and 836±32 from Behnke et al (Behnke et al., 1997). Due to the lack of aerosol inorganic composition (e.g., NH_4^+, NO_3^-, and SO_4^{2-}) measurements during the 2023 campaign, we estimated the range of $[Cl^-]/[H_2O]$ ratio from January to March in 2022 Delhi when ACSM measurements were available (Ali et al., 2025), where the chloride level was similar to the campaign in 2023. The estimated nocturnal (18:00~06:00) $[Cl^-]/[H_2O]$ ratio ranged from 1.8×10^{-5} to 0.76 with an average of 0.07, which mostly fell in the region where the corresponding $ClNO_2$ yield is close to 1 (Fig. S13a). We therefore tested the validity of the RH parameterization method by simulating the average nocturnal variation of $ClNO_2$ constrained with the parameterized gamma, observed N_2O_5 mixing ratios and aerosol surface area concentrations, with the $ClNO_2$ yield set to 1. The results showed that the simulation largely overestimated the production of $ClNO_2$ from 20:00 to 00:00 (Fig. S13b) when the absolute chloride levels were

relatively low (Fig. 1d). By comparison, when constraining $ClNO_2$ yield to 0 for the chloride-deficient period (20:00 to 00:00) and 1 for the chloride-sufficient period (0:00 to 6:00), the modelled $ClNO_2$ evolution well tracked the observations (Fig. S13b). The overall consistency between modelling and observations suggests that the measured $ClNO_2$ can largely explained by the locally heterogeneous uptake of N_2O_5 on chloride-rich particles and that the RH-parameterized $\gamma_{N_2O_5}$ is a reasonable estimate, indicating the key role of RH and thereby aerosol liquid water content in driving N_2O_5 uptake in Delhi. Nevertheless, comprehensive aerosol composition measurements or direct measurements of N_2O_5 reactivity (Bertram et al., 2009;Li et al., 2025) in future studies are required to enable better quantification and understanding N_2O_5 uptake processes in Delhi.

Table S1 Summary of the bulk PM composition measured at IITD during winter from 2017 to 2022. The unit is μg/m^3.

Period	PM	Cl	NO_3	SO_4	NH_4	Org	ref
2017.1~2017.3	PM_1	14.2	16.1	15.8	15.7	81.0	(Gani et al., 2019)
2017.12~2018.3	PM_1	18.9	19.6	11.1	15.9	99.9	(Gani et al., 2019)
2018.1.17~1.19 2018.2.5~3.11	$PM_{2.5}$	20.4	13.3	12.0	14.3	65.3	(Lalchandani et al., 2021)
2019.1.11~2.5	PM_1	17.3	20.8	18.0	23.7	80.0	(Haslett et al., 2023)
2019.12.1~2020.1.5	$PM_{2.5}$	5.7	14.5	11.4	9.5	60.9	(Ali et al., 2023)
2020.2.1~3.20	PM_1	4.9	10.6	9.7	8.9	47.9	(Mandariya et al., 2024)
2020.12.15~12.31	$PM_{2.5}$	11.3	27.2	13.7	25.7	111.5	(Faisal et al., 2025)
2020.12.15~2021.2.23	$PM_{2.5}$	4.9	19.8	15.5	15.7	96.2	(Ali et al., 2023)
2021.1.1~2021.2.28	$PM_{2.5}$	10.1	16.1	12.1	19.0	87.0	(Faisal et al., 2025)
2022.1.12~3.31	$PM_{2.5}$	4.5	15.3	14.0	12.9	86.2	(Ali et al., 2025)

Table S2 Campaign-averaged (both daytime and nighttime data are included) NO_3· reactivity (unit: s^{-1}) during the 2019 and 2023 campaign.

	NO_3 + NO	NO_3 + hv	N_2O_5 hete.	NO_3 + VOCs
2019.1~2	50.175	0.031	0.462	0.081
2023.2~3	15.585	0.043	0.091	0.081*

*It is assumed to be the same as those observed in 2019.

Table S3 Summary of nocturnal peak and average (shown in the brackets) N_2O_5 and $ClNO_2$ mixing ratios measured around the world. The unit is ppt.

Location	Period	Type	N_2O_5	$ClNO_2$	ref.
India Institute of Technology, Delhi	2023.2.23-3.14	urban inland	566 (16)	1340 (116)	this study
India Institute of Technology, Delhi	2019.1.11-2.5	urban inland	203 (4)	724 (48)	(Haslett et al., 2023)
Gulf of Mexico, Huston, Texas	2006.7-9	urban coastal	750	1200	(Osthoff et al., 2008)
National Oceanic and Atmospheric Administration, Boulder, Colorado	2009.2.11-2.25	urban inland	1500	440	(Thornton et al., 2010)
University of Utah, Salt Lake City, Utah	2015.12-2016.2	urban inland	1520 (76)		(Baasandorj et al., 2017)
University of Michigan, Ann Arbor, Michigan	2016.2.1-3.10	urban inland		220	(McNamara et al., 2020)
Toronto	2021.1.11-1.25	urban inland		300	(Wang et al., 2023)
Kensington	2012.7 -8	urban inland	1700	724 (84)	(Bannan et al., 2015)
Manchester	2014.10-11	urban inland		506	(Priestley et al., 2018)
Frankfurt Observatory	2011.8-9	rural inland	3000	800	(Phillips et al., 2012)
China, Wangdu	2014.6-7	rural inland	500	2070	(Tham et al., 2016)
China, Wangdu	2017.12	rural inland	1000	1400	(Xia et al., 2021)
China, Wangdu	2023.2.10-3.5	rural inland		3600	(Chen et al., 2025)
China, mountain in Hong Kong	2013.11-12	mountain site	7700	4700	(Wang et al., 2016)
China, Heshan	2017.1.2-1.15	urban coastal	3000	8300	(Chen et al., 2023)

Table S4 Average emission factor (g/kg fuel burned) of K, HCl, HCN, CO, and SO_2 from biomass, biofuel, and garbage burning processes and vehicles.

		K	HCl	HCN	SO_2	CO	HCl/CO	ref
Biomass burning	Peat	0.004~0.015	-	1.00	-	38	-	(Andreae, 2019)
	Crop residues	0.48	0.18	0.42	0.8	77	2.3×10^{-3}	(Andreae, 2019)
	Rice straw	-	0.44	0.37	1.3	60	7.3×10^{-3}	(Stockwell et al., 2014)
	Wheat straw	-	0.47	0.10	0.7	39	1.2×10^{-2}	(Stockwell et al., 2014)
	Tropical forest	0.32	0.13	0.44	0.8	104	1.3×10^{-3}	(Andreae, 2019)
	Temperate forest	0.18	0.04	0.64	0.7	112	3.5×10^{-4}	(Andreae, 2019)
Biofuel burning	Dung	0.09	0.04	1.30	0.7	89	4.3×10^{-4}	(Andreae, 2019)
	Biofuels without dung	0.13	0.08	0.39	0.5	84	8.9×10^{-4}	(Andreae, 2019)
	Charcoal	0.75	0.11	-	0.6	207	5.3×10^{-4}	(Andreae, 2019)
	Wood	-	0.02	0.54	bld	77	2.4×10^{-4}	(Stockwell et al., 2016)
Garbage burning	Garbage	0.02	2.80	0.43	0.5	66	4.2×10^{-2}	(Andreae, 2019)
	Mixed plastic garbage	-	2.30	0.43	bld	85	2.7×10^{-2}	(Stockwell et al., 2016)
Vehicles	Two-wheeled vehicles	-	bld	0.68	bld	761	-	(Stockwell et al., 2016)
	Agricultural irrigation pumps	-	bld	0.12	bld	17	-	(Stockwell et al., 2016)

Note: bld indicates below the limit of detection.

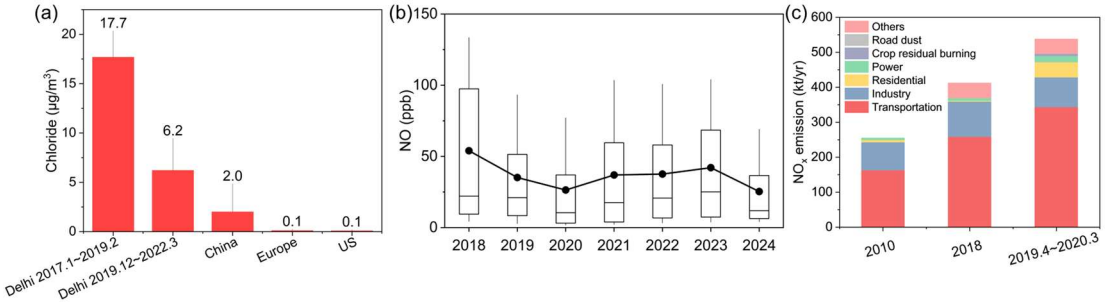

Fig. S1 Atmospheric chloride and NO concentrations and NO emissions in Delhi. (a) Comparison of the observed chloride levels globally. (b) Box plots of the annual daily averages of NO concentrations in Delhi. (c) NO_x emissions in Delhi from the year of 2010 (Beig, 2010), 2018 (Beig, 2018) and 2019.4~2020.3 (Sahu et al., 2023). The chloride concentrations in Delhi (compiled from Table S1), China (Xia et al., 2021;Tham et al., 2018;Xia et al., 2020), Europe (Eger et al., 2019;Lanz et al., 2010), and US (Mielke et al., 2013;Sarwar et al., 2012) are campaign-average values retrieved from previous studies. The whiskers in (a) represent standard deviation. The NO concentrations shown in (b) were obtained from the R.K. Puram monitoring station. The boxes represent the interquartile range with the whiskers extending to the 10th and 90th percentiles. The dot and horizontal line within each box denote the mean and median values, respectively.

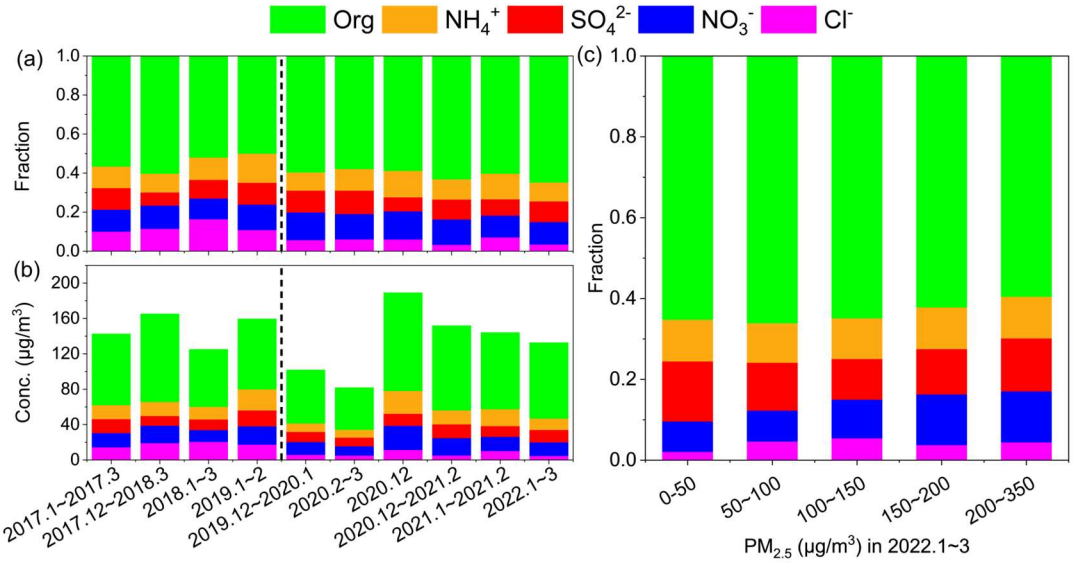

Fig. S2 (a-b) Temporal trends in bulk PM composition measured at IITD during winter from 2017 to 2022. (c) Variations of the composition fractions under varying $PM_{2.5}$ ranges. The original data for (a-b) was compiled from previous studies based on ACSM or AMS measurements and shown in Table S1. The dashed vertical line in (a-b) indicates the end of 2019. The $PM_{2.5}$ composition data in (c) was retrieved from Ali et al(Ali et al., 2025). and the corresponding $PM_{2.5}$ mass concentrations were obtained from the nearby R.K. Puram station.

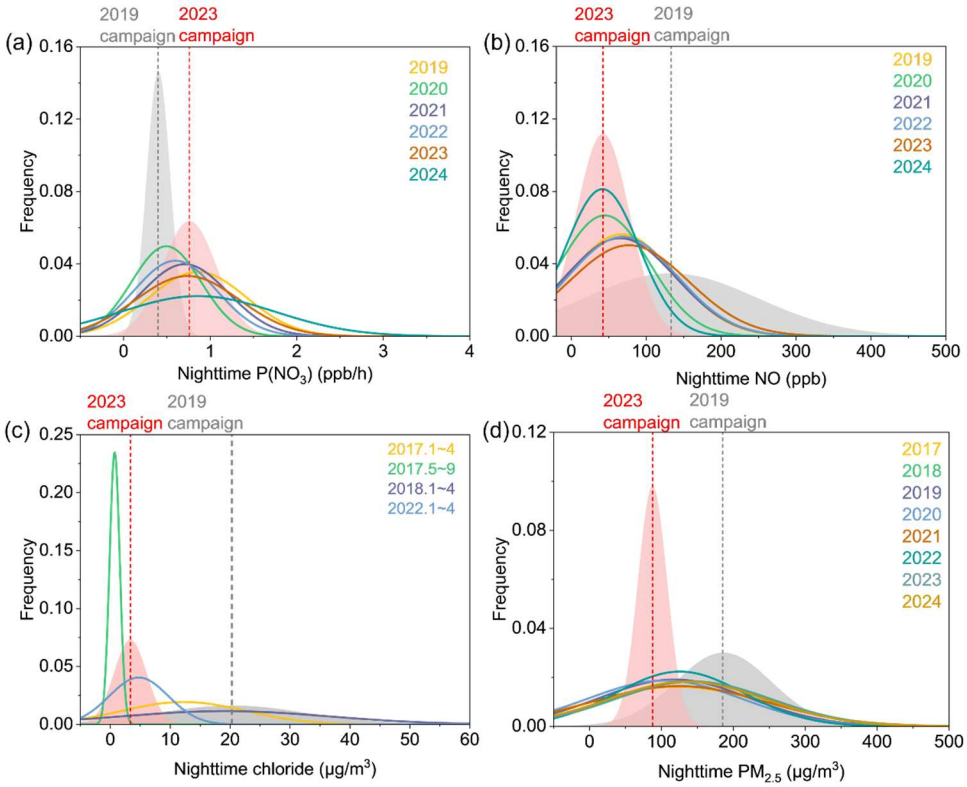

213

214 **Fig. S3 Representativeness of the two field-campaigns in Delhi.** Gaussian-fitted
215 frequency distributions of nightly (a) $P(NO_3)$, (b) NO, (c) chloride, and (d) $PM_{2.5}$
216 concentrations from 2017 to 2024. The nighttime is defined as 20:00~04:00 throughout
217 the years. The data for $P(NO_3)$, NO, and $PM_{2.5}$, are obtained from the R.K. Puram
218 monitoring station. Chloride concentrations were unavailable at the station and are
219 retrieved from previous studies (Gani et al., 2019;Ali et al., 2025). The gray and red
220 shaded area denote the respective pollutant distribution during the 2019 and 2023
221 campaign and the dashed lines indicate the campaign averages.

222

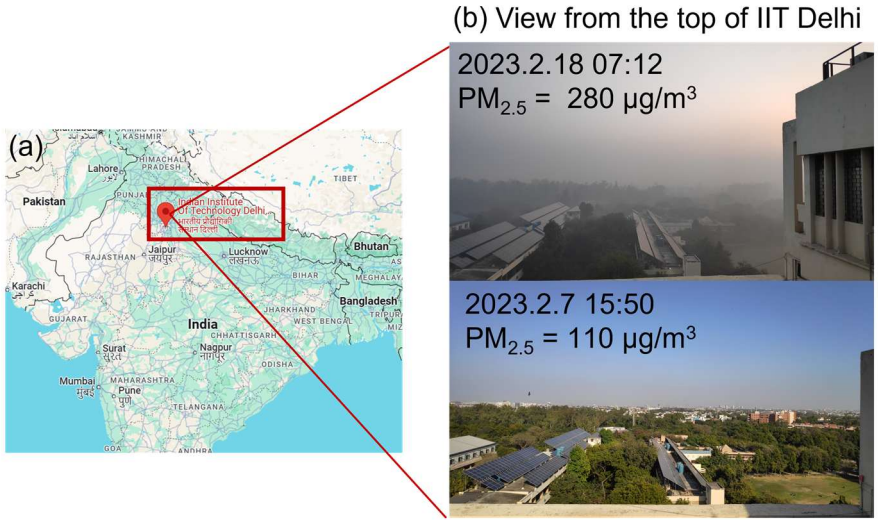

223

224 **Fig. S4 (a) The locations and (b) a zoom-in view of the sampling site**. The two photos
225 in (b) were taken during the early morning and late afternoon hours, respectively. The
226 map presented in panel (a) is credited to Google Maps.

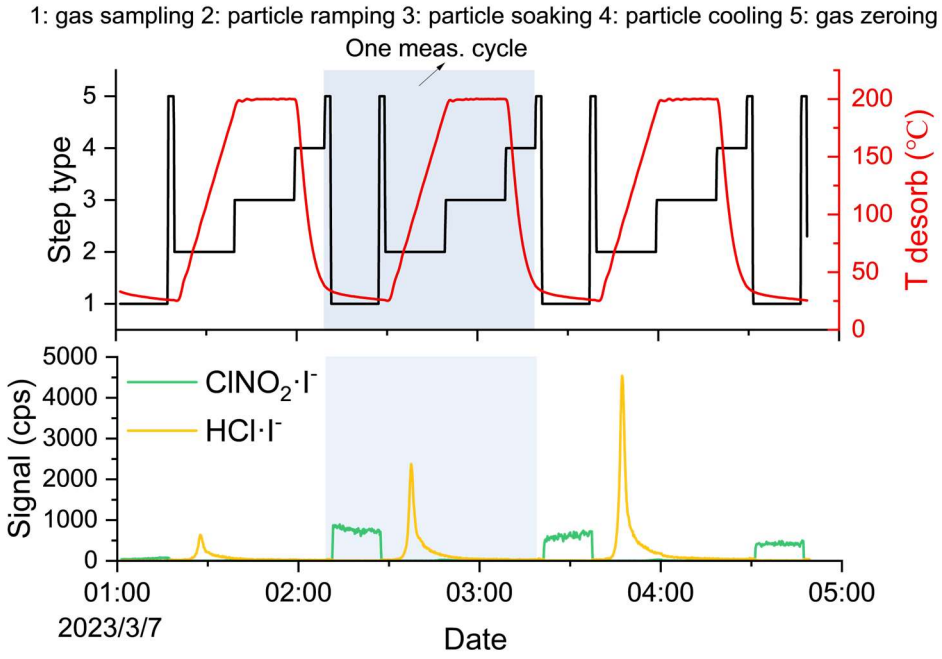

227

228 **Fig. S5 An example of the measurement cycle.**

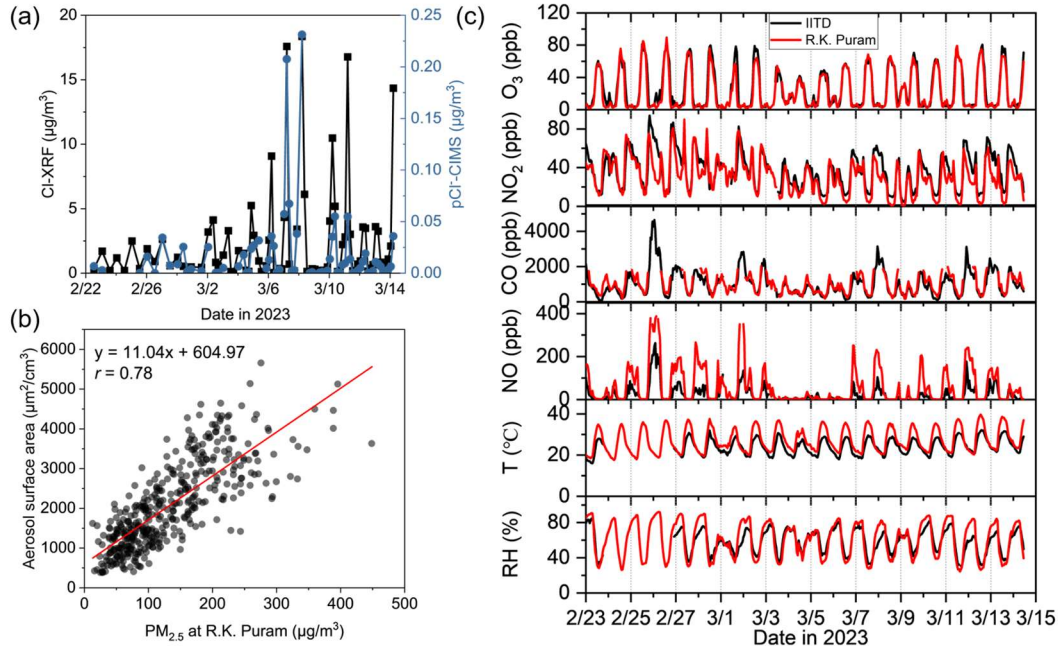

229

230 **Fig. S6 Intercomparison of the measured species and estimation of aerosol surface**
231 **area.** (a) Time series of particulate Cl measured by XRF and CIMS. (b) Correlation
232 between the measured aerosol surface area at IIT Delhi(Gani et al., 2020) and $PM_{2.5}$ at
233 R.K. Puram station from February to March in 2018. (c) Comparison of the time series
234 of trace gases and meteorological parameters measured at IIT Delhi and the R.K. Puram
235 station in 2023 campaign.

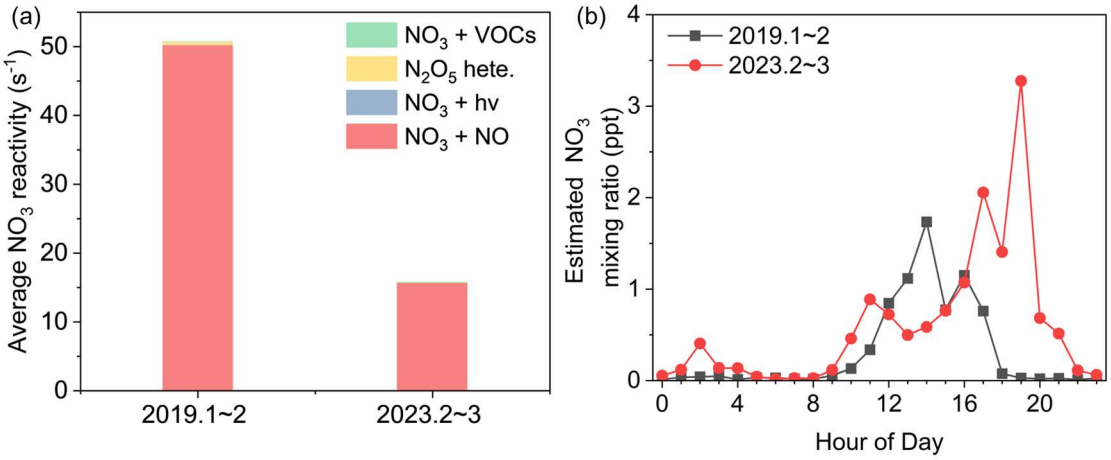

236

237 **Fig. S7 Loss of NO_3· and NO_3· mixing ratios.** (a) Campaign-averaged NO_3· reactivity
238 and (b) diuranl pattern of estimated NO_3· mixing ratios. The NO_3 mixing ratio was
239 estimated by using the observed N_2O_5 and NO_2 mixing ratio and the temperature-
240 dependent equilibrium constant between NO_2, NO_3, and N_2O_5.

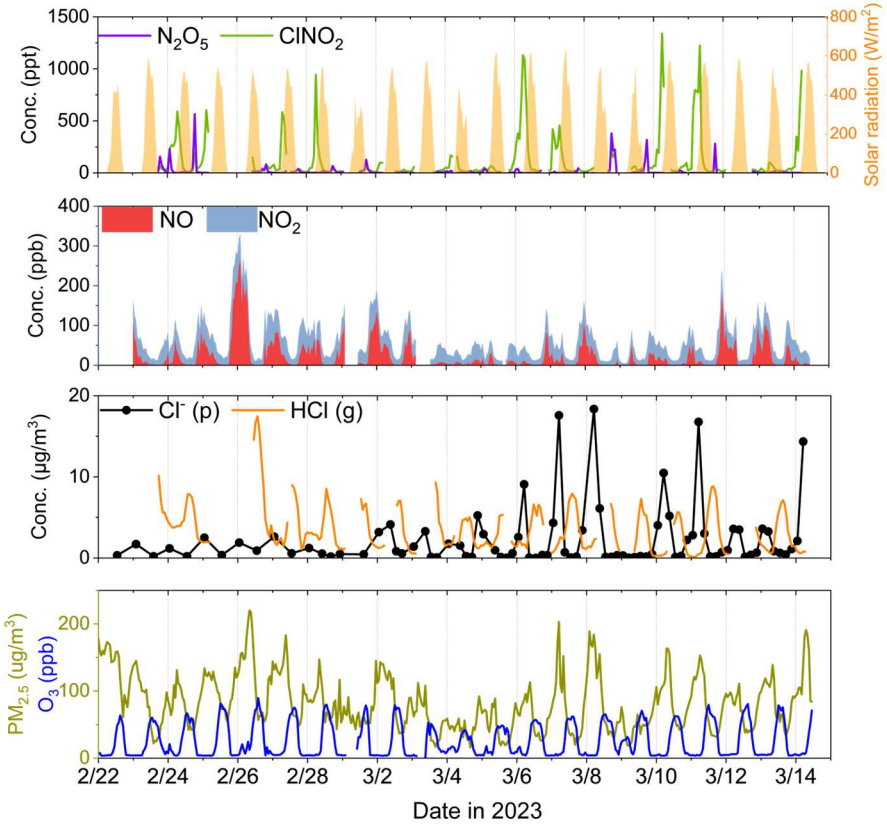

241

242 **Fig. S8 Overview of the field observations.** Time series of N_2O_5, $ClNO_2$, solar
243 radiation, NO, NO_2, gaseous HCl, $PM_{2.5}$, and O_3, and Cl element concentrations in
244 $PM_{2.5}$.

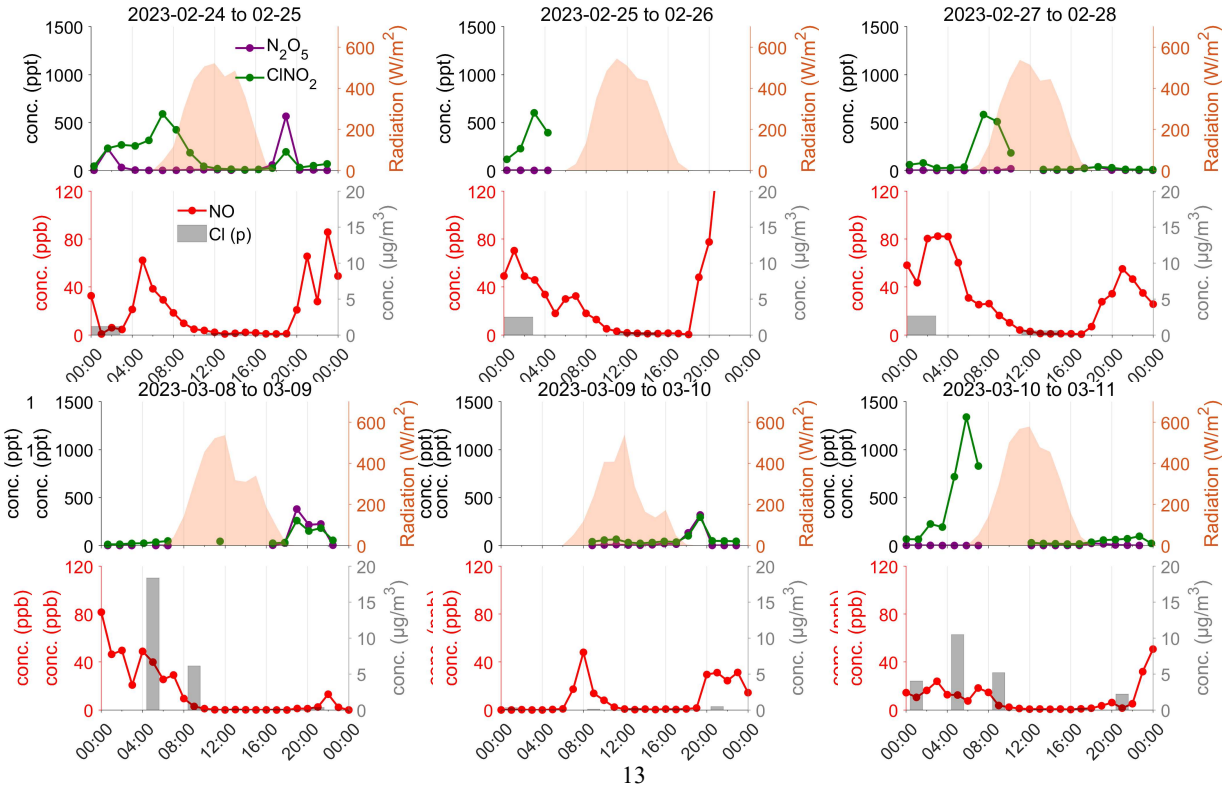

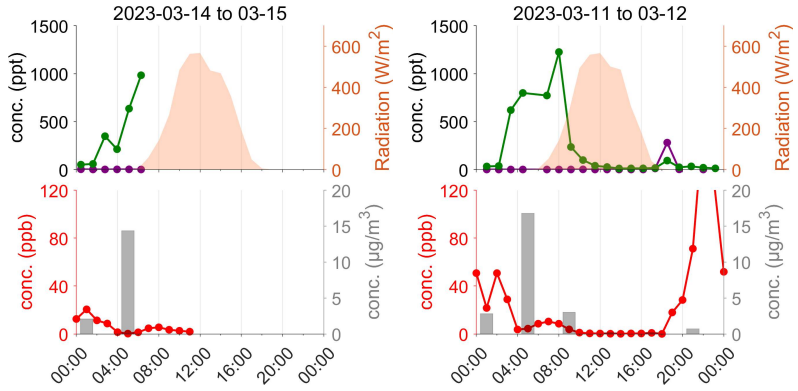

Fig. S9 Day by day plots of the enhanced cases observed in 2023. An enhanced case is identified by a pronounced nighttime increase in either N_2O_5 or $ClNO_2$.

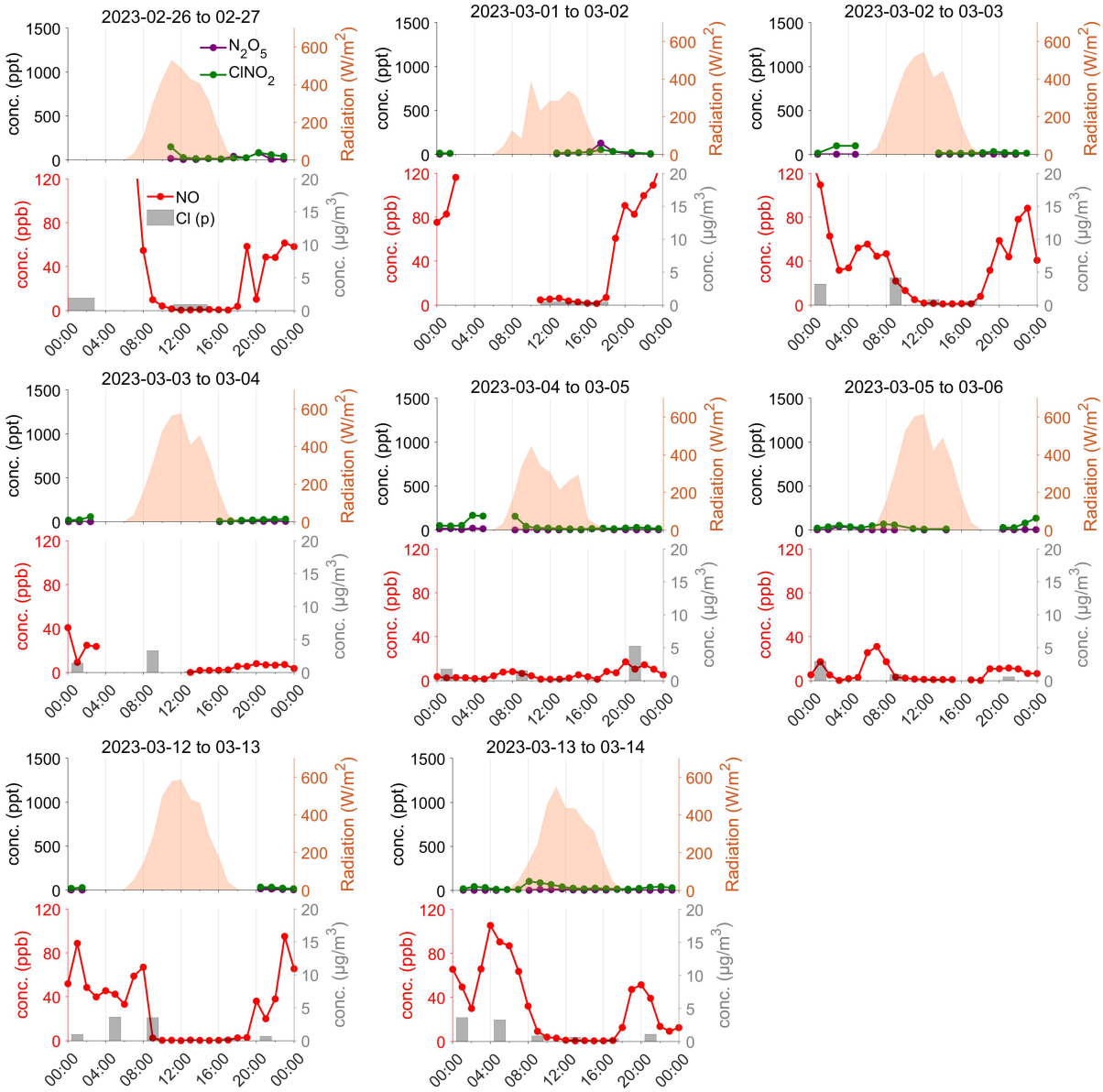

Fig. S10 Day by day plots of the non-enhanced cases observed in 2023. A non-

enhanced case is identified when neither N_2O_5 nor $ClNO_2$ shows a pronounced nighttime increase.

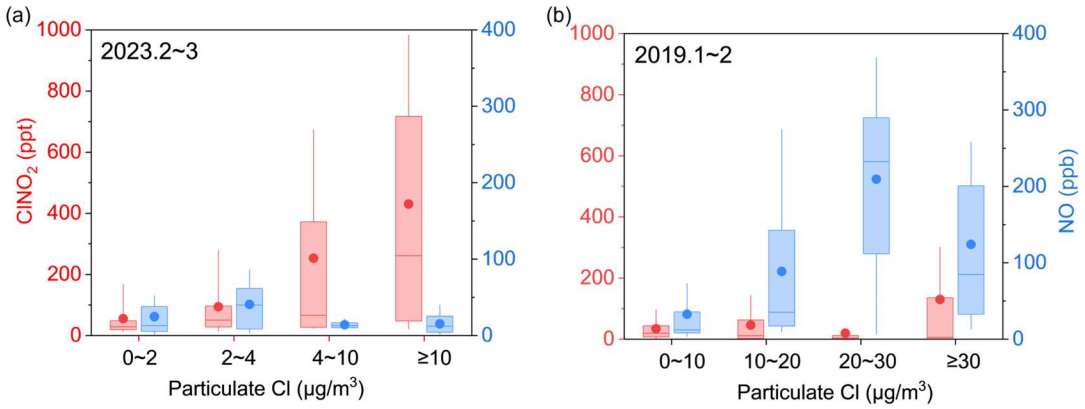

Fig. S11 Dependence of nocturnal $ClNO_2$ on chloride and NO during the (a) 2023 and (b) 2019 campaign. $ClNO_2$ and NO were stratified by chloride concentration intervals. Boxes and whiskers represent 25th and 75th , 10th and 90th percentiles, respectively. The dots and lines inside the box denote average and median values.

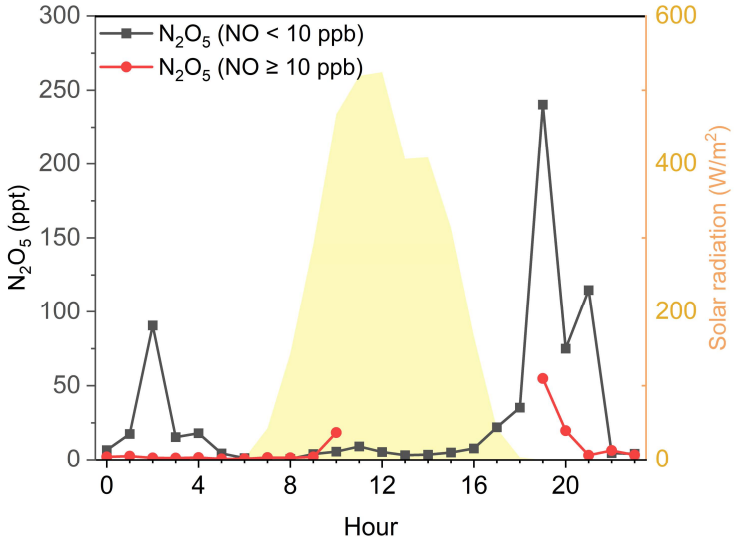

Fig. S12 Average diurnal variations of (a) N_2O_5 under low- and high-NO conditions (b) $PM_{2.5}$, total measured gaseous and particulate organics in 2023. A 10 ppb of NO threshold was applied to ensure statistically robust and comparable datasets. As all NO concentrations were below 10 ppb between 11:00 and 18:00, no N_2O_5 data are available for the high-NO condition during this period. The right axis in (b) shows the average solar radiation in 2023.

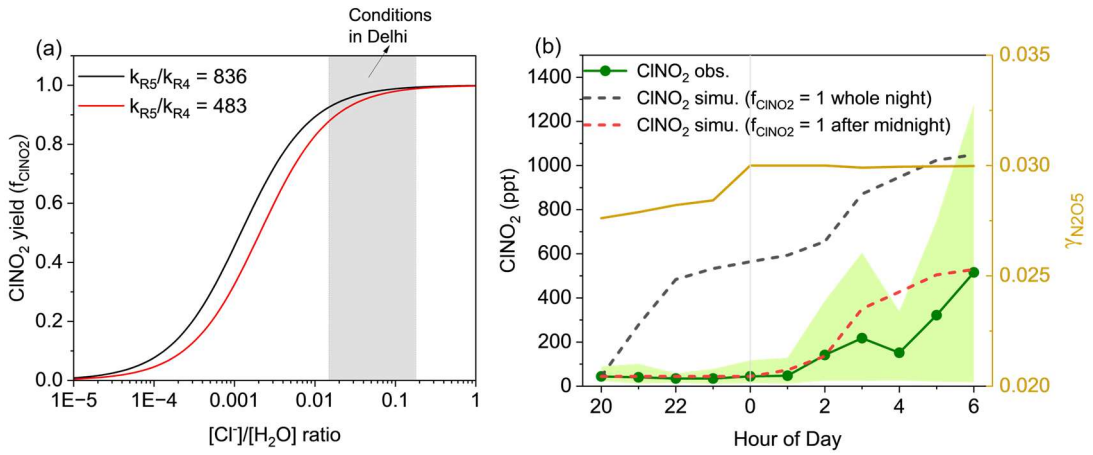

Fig. S13 (a) Parameterization of $ClNO_2$ yield and (b) simulation of the nocturnal $ClNO_2$ variations. The lines in (a) correspond to $ClNO_2$ yield calculated using Eq. 3 with different reported reaction rate constant ratios. The grey shaded area indicates the 10th and 90th percentiles of the calculated $[Cl^-]/[H_2O]$ ratios using ISORROPIA from January to March of 2022 in Delhi(Ali et al., 2025). The green shaded area in (b) represents the 10th and 90th percentiles of the observed average nocturnal $ClNO_2$ mixing ratios. The dashed lines in (b) are the simulated $ClNO_2$ mixing ratios and the average RH parameterized N_2O_5 uptake coefficient is shown in the right axis of (b).

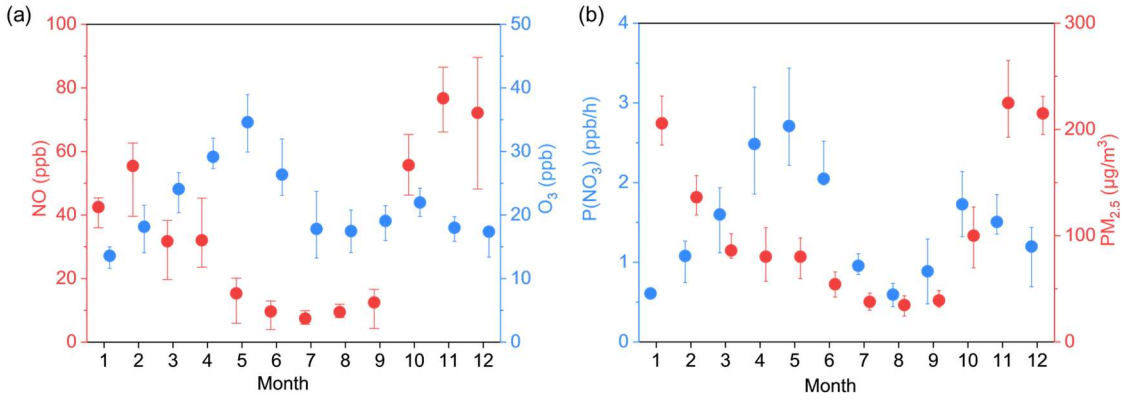

Fig. S14 Monthly variations of NO, O_3, $P(NO_3)$, and $PM_{2.5}$ in Delhi. Average monthly variations of (a) NO and O_3 and (b) $P(NO_3)$ and $PM_{2.5}$ from 2017 to 2024. The dots represent the averages and the whiskers denote the 25th to 75th percentile ranges. All data were obtained from the R.K. Puram national monitoring station.

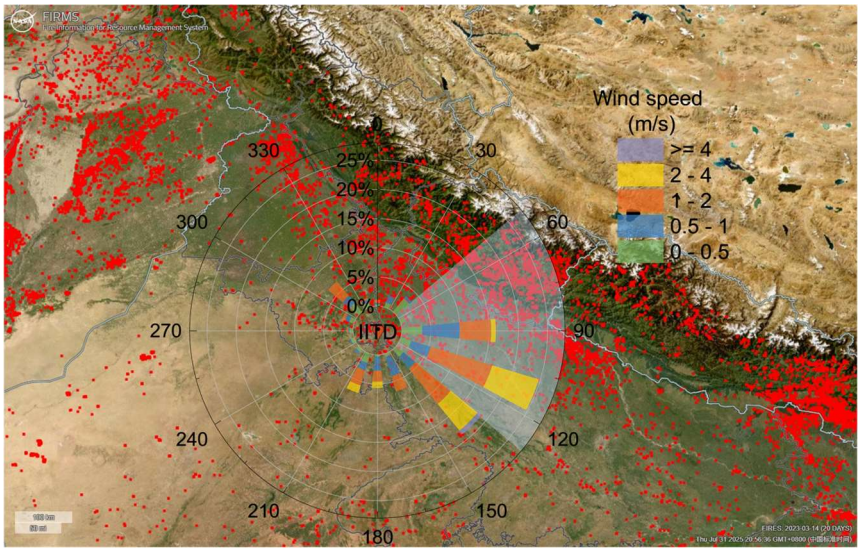

278

279 **Fig. S15 Satellite observations of active fire hotspots and wind rose plot during the**
280 **2023 campaign.** The map of the fire-points was downloaded from NASA FIRMS active
281 fire data (https:// earthdata.nasa.gov/firms). The measurement site (IIT Delhi) was
282 indicated as IITD. The light blue shaded area indicates the dominant wind-direction
283 (50~130°) when the extremely high values of the uptake parameter (γ×f) exceeding 0.1
284 were measured.

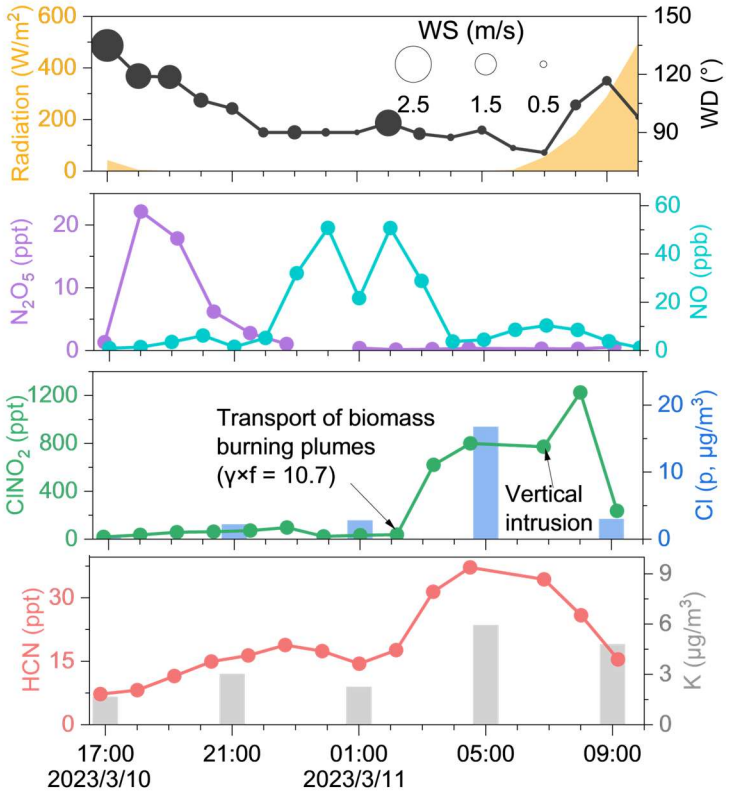

285

286 **Fig. S16 A case study indicating the influence of transport on the observed $ClNO_2$**
287 **levels.** An exceptionally high γ×f value (10.7) observed at 2023/3/11 2:10 is also noted.

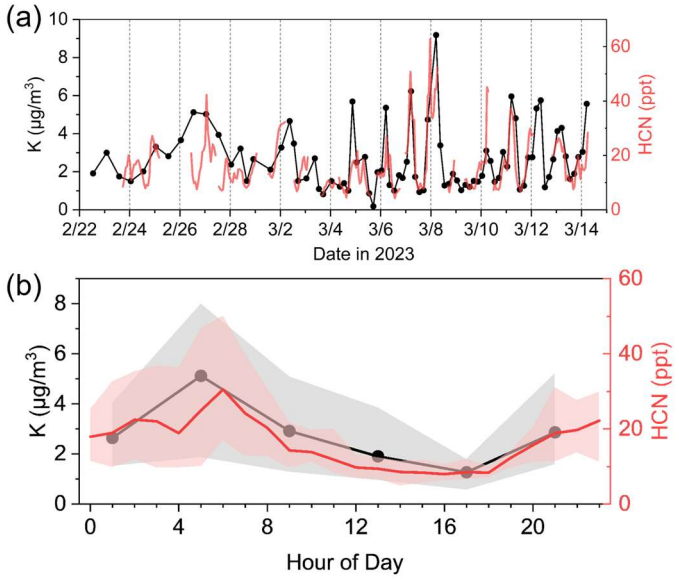

Fig. S17 (a) Time series and (b) average diurnal pattern of element K and gaseous HCN during the 2023 campaign. The shaded areas indicates 10th and 90th percentiles and the lines represent the campaign-averaged values. Hourly CIMS measurements were shown for HCN. The highest K and HCN concentrations on 3/7 and 3/8 were likely driven by large-scale bonfires involving wood and leaves burning during the Holika Dahan festival (3/6 16:00~3/8).

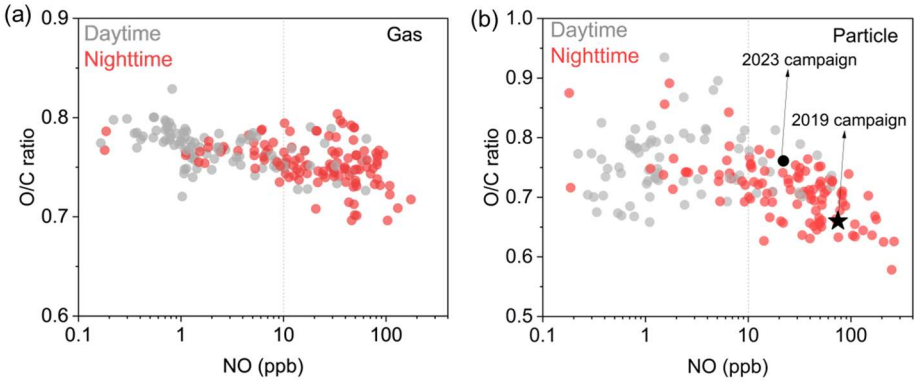

Fig. S18 NO dependence of the gaseous and particulate bulk O/C ratio in Delhi. Scatter plots showing the relationship between ambient NO levels and concentration-weighted bulk O/C ratios in the (a) gas and (b) particle phases.

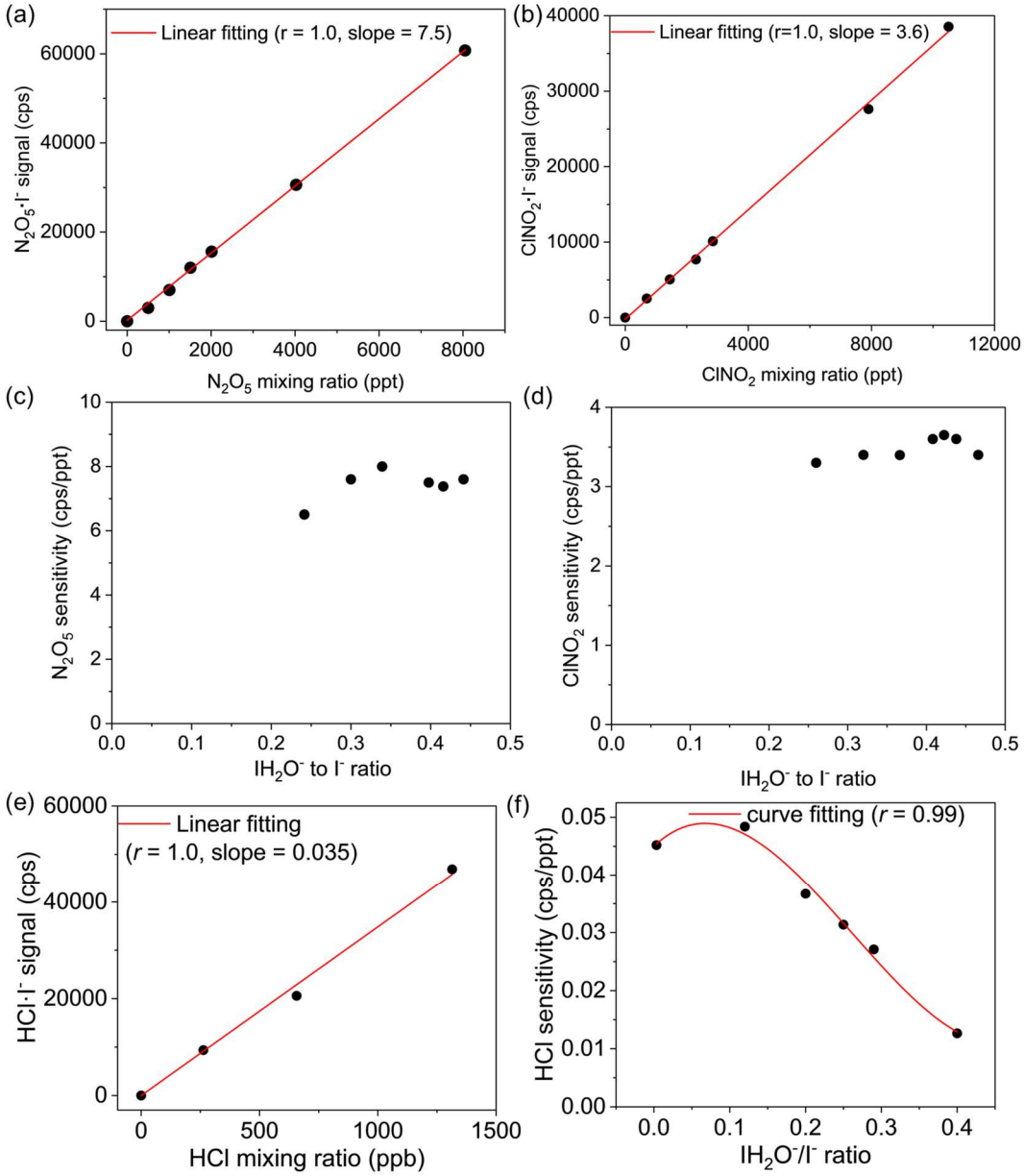

305

306 **Fig. S19 Sensitivity calibrations for gaseous (a) N_2O_5, (b) $ClNO_2$, and (e) HCl, and**
307 **the water dependence of the sensitivities of (c) N_2O_5, (d) $ClNO_2$, and (f) HCl.** Multi-
308 point calibrations for N_2O_5 and $ClNO_2$ were performed under RH conditions
309 corresponding to an IH_2O^- to I^- ratio of 0.42 ± 0.02, while the calibration curve at an
310 $I{\cdot}H_2O^-$ to I^- ratio of 0.19 was shown for HCl.

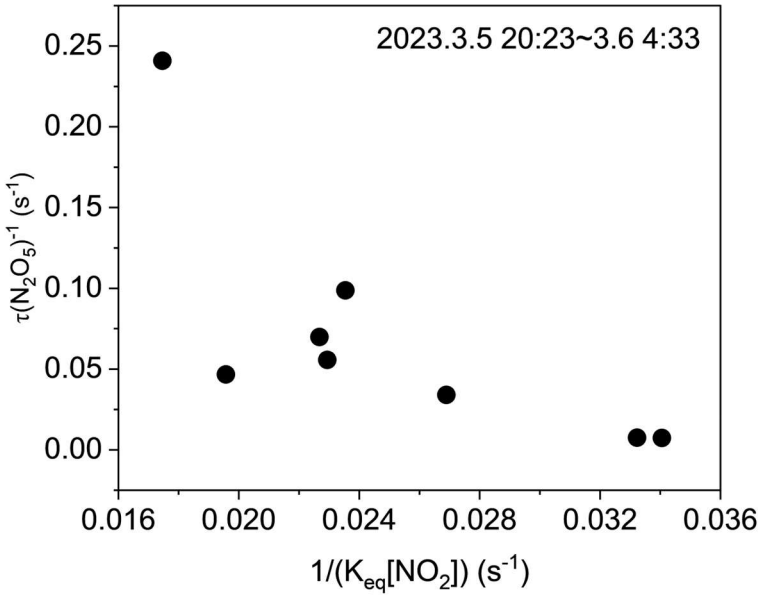

Fig. S20 An example of the steady-state analysis of the NO_2-NO_3-N_2O_5 system.

References

Ali, U., Faisal, M., Ganguly, D., Kumar, M., and Singh, V.: Analysis of aerosol liquid water content and its role in visibility reduction in Delhi, Science of the Total Environment, 867, 161484, https://doi.org/https://doi.org/10.1016/j.scitotenv.2023.161484, 2023.

Ali, U., Singh, V., Faisal, M., Kumar, M., and Gani, S.: Exploring the influence of physical and chemical factors on new particle formation in a polluted megacity, Environmental Science: Atmospheres, 5, 25–47, https://doi.org/10.1039/D4EA00114A, 2025.

Andreae, M. O.: Emission of trace gases and aerosols from biomass burning - an updated assessment, Atmospheric Chemistry and Physics, 19, 8523–8546, https://doi.org/10.5194/acp-19-8523-2019, 2019.

Baasandorj, M., Hoch, S. W., Bares, R., Lin, J. C., Brown, S. S., Millet, D. B., Martin, R., Kelly, K., Zarzana, K. J., Whiteman, C. D., Dube, W. P., Tonnesen, G., Jaramillo, I. C., and Sohl, J.: Coupling between chemical and meteorological processes under persistent cold-air pool conditions: Evolution of wintertime $PM_{2.5}$ pollution events and N_2O_5 observations in Utah's salt lake valley, Environmental Science & Technology, 51, 5941–5950, https://doi.org/10.1021/acs.est.6b06603, 2017.

Bannan, T. J., Booth, A. M., Bacak, A., Muller, J. B. A., Leather, K. E., Le Breton, M., Jones, B., Young, D., Coe, H., Allan, J., Visser, S., Slowik, J. G., Furger, M., Prévôt, A. S. H., Lee, J., Dunmore, R. E., Hopkins, J. R., Hamilton, J. F., Lewis, A. C., Whalley, L. K., Sharp, T., Stone, D., Heard, D. E., Fleming, Z. L., Leigh, R., Shallcross, D. E., and Percival, C. J.: The first UK measurements of nitryl chloride using a chemical

ionization mass spectrometer in central London in the summer of 2012, and an investigation of the role of Cl atom oxidation, Journal of Geophysical Research: Atmospheres, 120, 5638–5657, https://doi.org/10.1002/2014jd022629, 2015.

Behnke, W., George, C., Scheer, V., and Zetzsch, C.: Production and decay of $ClNO_2$ from the reaction of gaseous N_2O_5 with NaCl solution: Bulk and aerosol experiments, Journal of Geophysical Research: Atmospheres, 102, 3795–3804, https://doi.org/https://doi.org/10.1029/96JD03057, 1997.

Beig, G.: SAFAR-Delhi-2010: Development of high resolution emission inventory for National Capital Region Delhi, Indian Institute of Tropical Meteorology (IITM), 2010.

Beig, G.: SAFAR-Delhi-2018: SAFAR-High Resolution Emission Inventory of Megacity Delhi 2018, Indian Institute of Tropical Meteorology (IITM), 2018.

Bertram, T. H., and Thornton, J. A.: Toward a general parameterization of N_2O_5 reactivity on aqueous particles: the competing effects of particle liquid water, nitrate and chloride, Atmospheric Chemistry and Physics, 9, 8351–8363, https://doi.org/10.5194/acp-9-8351-2009, 2009.

Bertram, T. H., Thornton, J. A., and Riedel, T. P.: An experimental technique for the direct measurement of N_2O_5 reactivity on ambient particles, Atmospheric Measurement Techniques, 2, 231–242, https://doi.org/10.5194/amt-2-231-2009, 2009.

Brown, S. S., Stark, H., and Ravishankara, A. R.: Applicability of the steady state approximation to the interpretation of atmospheric observations of NO_3 and N_2O_5, Journal of Geophysical Research: Atmospheres, 108, https://doi.org/https://doi.org/10.1029/2003JD003407, 2003.

Brown, S. S., Ryerson, T. B., Wollny, A. G., Brock, C. A., Peltier, R., Sullivan, A. P., Weber, R. J., Dubé, W. P., Trainer, M., Meagher, J. F., Fehsenfeld, F. C., and Ravishankara, A. R.: Variability in nocturnal nitrogen oxide processing and its role in regional air quality, Science, 311, 67–70, https://doi.org/doi:10.1126/science.1120120, 2006.

Chen, X., Xia, M., Wang, W., Yun, H., Yue, D., and Wang, T.: Fast near-surface $ClNO_2$ production and its impact on O_3 formation during a heavy pollution event in South China, Science of the Total Environment, 858, 159998, https://doi.org/10.1016/j.scitotenv.2022.159998, 2023.

Chen, X., Jiang, Y., Zong, Z., Wang, Y., Sun, W., Wang, Y., Xia, M., Guan, L., Liu, P., Zhang, C., Chen, J., Mu, Y., and Wang, T.: Atmospheric reactive halogens reshaped by the clean energy policy and agricultural activity in a rural area of the north China plain, Environmental Science & Technology, 59, 12775–12785, https://doi.org/10.1021/acs.est.4c13986, 2025.

Eger, P. G., Friedrich, N., Schuladen, J., Shenolikar, J., Fischer, H., Tadic, I., Harder, H., Martinez, M., Rohloff, R., Tauer, S., Drewnick, F., Fachinger, F., Brooks, J., Darbyshire, E., Sciare, J., Pikridas, M., Lelieveld, J., and Crowley, J. N.: Shipborne measurements of $ClNO_2$ in the Mediterranean Sea and around the Arabian Peninsula during summer, Atmospheric Chemistry and Physics, 19, 12121–12140,

https://doi.org/10.5194/acp-19-12121-2019, 2019.

Faisal, M., Ali, U., Kumar, A., Kumar, M., and Singh, V.: Unveiling $PM_{2.5}$ sources: Double and tracer conjugate PMF approaches for high-resolution organic, BC, and inorganic $PM_{2.5}$ data, Atmospheric Environment, 343, 121011, https://doi.org/https://doi.org/10.1016/j.atmosenv.2024.121011, 2025.

Finlayson-Pitts, B. J.: The tropospheric chemistry of sea salt: A molecular-level view of the chemistry of NaCl and NaBr, Chemical Reviews, 103, 4801–4822, https://doi.org/10.1021/cr020653t, 2003.

Gani, S., Bhandari, S., Seraj, S., Wang, D. S., Patel, K., Soni, P., Arub, Z., Habib, G., Hildebrandt Ruiz, L., and Apte, J. S.: Submicron aerosol composition in the world's most polluted megacity: The Delhi Aerosol Supersite study, Atmospheric Chemistry and Physics, 19, 6843–6859, https://doi.org/10.5194/acp-19-6843-2019, 2019.

Gani, S., Bhandari, S., Patel, K., Seraj, S., Soni, P., Arub, Z., Habib, G., Hildebrandt Ruiz, L., and Apte, J. S.: Particle number concentrations and size distribution in a polluted megacity: the Delhi Aerosol Supersite study, Atmospheric Chemistry and Physics, 20, 8533–8549, https://doi.org/10.5194/acp-20-8533-2020, 2020.

Haslett, S. L., Bell, D. M., Kumar, V., Slowik, J. G., Wang, D. S., Mishra, S., Rastogi, N., Singh, A., Ganguly, D., Thornton, J., Zheng, F., Li, Y., Nie, W., Liu, Y., Ma, W., Yan, C., Kulmala, M., Daellenbach, K. R., Hadden, D., Baltensperger, U., Prevot, A. S. H., Tripathi, S. N., and Mohr, C.: Nighttime NO emissions strongly suppress chlorine and nitrate radical formation during the winter in Delhi, Atmospheric Chemistry and Physics, 23, 9023–9036, https://doi.org/10.5194/acp-23-9023-2023, 2023.

Lalchandani, V., Kumar, V., Tobler, A., M. Thamban, N., Mishra, S., Slowik, J. G., Bhattu, D., Rai, P., Satish, R., Ganguly, D., Tiwari, S., Rastogi, N., Tiwari, S., Močnik, G., Prévôt, A. S. H., and Tripathi, S. N.: Real-time characterization and source apportionment of fine particulate matter in the Delhi megacity area during late winter, Science of the Total Environment, 770, 145324, https://doi.org/https://doi.org/10.1016/j.scitotenv.2021.145324, 2021.

Lanz, V. A., Prévôt, A. S. H., Alfarra, M. R., Weimer, S., Mohr, C., DeCarlo, P. F., Gianini, M. F. D., Hueglin, C., Schneider, J., Favez, O., D'Anna, B., George, C., and Baltensperger, U.: Characterization of aerosol chemical composition with aerosol mass spectrometry in Central Europe: An overview, Atmospheric Chemistry and Physics, 10, 10453–10471, https://doi.org/10.5194/acp-10-10453-2010, 2010.

Lee, B. H., Lopez-Hilfiker, F. D., Mohr, C., Kurten, T., Worsnop, D. R., and Thornton, J. A.: An iodide-adduct high-resolution time-of-flight chemical-ionization mass spectrometer: Application to atmospheric inorganic and organic compounds, Environmental Science & Technology, 48, 6309–6317, https://doi.org/10.1021/es500362a, 2014.

Li, J., Zhai, T., Chen, X., Wang, H., Xie, S., Chen, S., Li, C., Gong, Y., Dong, H., and Lu, K.: Direct measurement of N_2O_5 heterogeneous uptake coefficients on

atmospheric aerosols in southwestern China and evaluation of current parameterizations, Atmos. Chem. Phys., 25, 6395–6406, https://doi.org/10.5194/acp-25-6395-2025, 2025.

Mandariya, A. K., Ahlawat, A., Haneef, M., Baig, N. A., Patel, K., Apte, J., Hildebrandt Ruiz, L., Wiedensohler, A., and Habib, G.: Measurement report: Hygroscopicity of size-selected aerosol particles in the heavily polluted urban atmosphere of Delhi: Impacts of chloride aerosol, Atmospheric Chemistry and Physics, 24, 3627–3647, https://doi.org/10.5194/acp-24-3627-2024, 2024.

McNamara, S. M., Kolesar, K. R., Wang, S., Kirpes, R. M., May, N. W., Gunsch, M. J., Cook, R. D., Fuentes, J. D., Hornbrook, R. S., Apel, E. C., China, S., Laskin, A., and Pratt, K. A.: Observation of road salt aerosol driving inland wintertime atmospheric chlorine chemistry, ACS Central Science, 6, 684–694, https://doi.org/10.1021/acscentsci.9b00994, 2020.

Mielke, L. H., Stutz, J., Tsai, C., Hurlock, S. C., Roberts, J. M., Veres, P. R., Froyd, K. D., Hayes, P. L., Cubison, M. J., Jimenez, J. L., Washenfelder, R. A., Young, C. J., Gilman, J. B., Gouw, J. A., Flynn, J. H., Grossberg, N., Lefer, B. L., Liu, J., Weber, R. J., and Osthoff, H. D.: Heterogeneous formation of nitryl chloride and its role as a nocturnal NO_x reservoir species during CalNex-LA 2010, Journal of Geophysical Research: Atmospheres, 118, 10638–10652, https://doi.org/10.1002/jgrd.50783, 2013.

Osthoff, H. D., Roberts, J. M., Ravishankara, A. R., Williams, E. J., Lerner, B. M., Sommariva, R., Bates, T. S., Coffman, D., Quinn, P. K., Dibb, J. E., Stark, H., Burkholder, J. B., Talukdar, R. K., Meagher, J., Fehsenfeld, F. C., and Brown, S. S.: High levels of nitryl chloride in the polluted subtropical marine boundary layer, Nature Geoscience, 1, 324–328, https://doi.org/10.1038/ngeo177, 2008.

Phillips, G. J., Tang, M. J., Thieser, J., Brickwedde, B., Schuster, G., Bohn, B., Lelieveld, J., and Crowley, J. N.: Significant concentrations of nitryl chloride observed in rural continental Europe associated with the influence of sea salt chloride and anthropogenic emissions, Geophysical Research Letters, 39, L10811, https://doi.org/10.1029/2012gl051912, 2012.

Priestley, M., le Breton, M., Bannan, T. J., Worrall, S. D., Bacak, A., Smedley, A. R. D., Reyes-Villegas, E., Mehra, A., Allan, J., Webb, A. R., Shallcross, D. E., Coe, H., and Percival, C. J.: Observations of organic and inorganic chlorinated compounds and their contribution to chlorine radical concentrations in an urban environment in northern Europe during the wintertime, Atmospheric Chemistry and Physics, 18, 13481–13493, https://doi.org/10.5194/acp-18-13481-2018, 2018.

Sahu, S. K., Mangaraj, P., and Beig, G.: Decadal growth in emission load of major air pollutants in Delhi, Earth System Science Data, 15, 3183–3202, https://doi.org/10.5194/essd-15-3183-2023, 2023.

Sarwar, G., Simon, H., Bhave, P., and Yarwood, G.: Examining the impact of heterogeneous nitryl chloride production on air quality across the United States, Atmospheric Chemistry and Physics, 12, 6455–6473, https://doi.org/10.5194/acp-12-6455-2012, 2012.

Stockwell, C. E., Yokelson, R. J., Kreidenweis, S. M., Robinson, A. L., DeMott, P. J., Sullivan, R. C., Reardon, J., Ryan, K. C., Griffith, D. W. T., and Stevens, L.: Trace gas emissions from combustion of peat, crop residue, domestic biofuels, grasses, and other fuels: Configuration and fourier transform infrared (FTIR) component of the fourth fire lab at missoula experiment (FLAME-4), Atmospheric Chemistry and Physics, 14, 9727–9754, https://doi.org/10.5194/acp-14-9727-2014, 2014.

Stockwell, C. E., Christian, T. J., Goetz, J. D., Jayarathne, T., Bhave, P. V., Praveen, P. S., Adhikari, S., Maharjan, R., DeCarlo, P. F., Stone, E. A., Saikawa, E., Blake, D. R., Simpson, I. J., Yokelson, R. J., and Panday, A. K.: Nepal ambient monitoring and source testing experiment (NAMaSTE): Emissions of trace gases and light-absorbing carbon from wood and dung cooking fires, garbage and crop residue burning, brick kilns, and other sources, Atmospheric Chemistry and Physics, 16, 11043–11081, https://doi.org/10.5194/acp-16-11043-2016, 2016.

Tham, Y. J., Wang, Z., Li, Q., Yun, H., Wang, W., Wang, X., Xue, L., Lu, K., Ma, N., Bohn, B., Li, X., Kecorius, S., Größ, J., Shao, M., Wiedensohler, A., Zhang, Y., and Wang, T.: Significant concentrations of nitryl chloride sustained in the morning: Investigations of the causes and impacts on ozone production in a polluted region of northern China, Atmospheric Chemistry and Physics, 16, 14959–14977, https://doi.org/10.5194/acp-16-14959-2016, 2016.

Tham, Y. J., Wang, Z., Li, Q., Wang, W., Wang, X., Lu, K., Ma, N., Yan, C., Kecorius, S., Wiedensohler, A., Zhang, Y., and Wang, T.: Heterogeneous N_2O_5 uptake coefficient and production yield of $ClNO_2$ in polluted northern China: Roles of aerosol water content and chemical composition, Atmospheric Chemistry and Physics, 18, 13155–13171, https://doi.org/10.5194/acp-18-13155-2018, 2018.

Thornton, J. A., Kercher, J. P., Riedel, T. P., Wagner, N. L., Cozic, J., Holloway, J. S., Dube, W. P., Wolfe, G. M., Quinn, P. K., Middlebrook, A. M., Alexander, B., and Brown, S. S.: A large atomic chlorine source inferred from mid-continental reactive nitrogen chemistry, Nature, 464, 271–274, https://doi.org/10.1038/nature08905, 2010.

Vohra, K., S, M., Chakraborty, A., Shah, H., As, B., and Pakki, J.: Urgent issues regarding real-time air quality monitoring data in India: Unveiling solutions and implications for policy and health, Atmospheric Environment: X, 25, 100308, https://doi.org/https://doi.org/10.1016/j.aeaoa.2024.100308, 2025.

Wang, C., Liggio, J., Wentzell, J. J. B., Jorga, S., Folkerson, A., and Abbatt, J. P. D.: Chloramines as an important photochemical source of chlorine atoms in the urban atmosphere, Proceedings of the National Academy of Sciences of the United States of America, 120, e2220889120, https://doi.org/doi:10.1073/pnas.2220889120, 2023.

Wang, T., Brown, S. S., Dubé, W. P., Tham, Y. J., Zha, Q., Xue, L., Poon, S., Wang, Z., Blake, D. R., Tsui, W., and Parrish, D. D.: Observations of nitryl chloride and modeling its source and effect on ozone in the planetary boundary layer of southern China, Journal of Geophysical Research: Atmospheres, 121, 2457–2475, https://doi.org/10.1002/2015jd024566, 2016.

Wang, X., Wang, H., Xue, L., Wang, T., Wang, L., Gu, R., Wang, W., Tham, Y. J.,

Wang, Z., Yang, L., Chen, J., and Wang, W.: Observations of N_2O_5 and $ClNO_2$ at a polluted urban surface site in North China: High N_2O_5 uptake coefficients and low $ClNO_2$ product yields, Atmospheric Environment, 156, 125–134, https://doi.org/10.1016/j.atmosenv.2017.02.035, 2017a.

Wang, Z., Wang, W., Tham, Y. J., Li, Q., Wang, H., Wen, L., Wang, X., and Wang, T.: Fast heterogeneous N2O5 uptake and ClNO2 production in power plant and industrial plumes observed in the nocturnal residual layer over the North China Plain, Atmos. Chem. Phys., 17, 12361–12378, https://doi.org/10.5194/acp-17-12361-2017, 2017b.

Xia, M., Peng, X., Wang, W., Yu, C., Sun, P., Li, Y., Liu, Y., Xu, Z., Wang, Z., Xu, Z., Nie, W., Ding, A., and Wang, T.: Significant production of $ClNO_2$ and possible source of Cl_2 from N_2O_5 uptake at a suburban site in eastern China, Atmospheric Chemistry and Physics, 20, 6147–6158, https://doi.org/10.5194/acp-20-6147-2020, 2020.

Xia, M., Peng, X., Wang, W., Yu, C., Wang, Z., Tham, Y. J., Chen, J., Chen, H., Mu, Y., Zhang, C., Liu, P., Xue, L., Wang, X., Gao, J., Li, H., and Wang, T.: Winter $ClNO_2$ formation in the region of fresh anthropogenic emissions: Seasonal variability and insights into daytime peaks in northern China, Atmospheric Chemistry and Physics, 21, 15985–16000, https://doi.org/10.5194/acp-21-15985-2021, 2021.

Xie, Y., Zhou, M., Hunt, K. M. R., and Mauzerall, D. L.: Recent $PM_{2.5}$ air quality improvements in India benefited from meteorological variation, Nature Sustainability, 7, 983–993, https://doi.org/10.1038/s41893-024-01366-y, 2024.